Lithos 380–381 (2021) 105880

Contents lists available at ScienceDirect

Lithos

journal homepage: www.elsevier.com/locate/lithos

Research Article

Siderophile and chalcophile elements in spinels, sulphides and native Ni in strongly metasomatised xenoliths from the Bultfontein kimberlite (South Africa)

Sonja Aulbach [a,**], Andrea Giuliani [b,c,*], Marco L. Fiorentini [d], Raphael J. Baumgartner [d,e,f], Dany Savard [g], Vadim S. Kamenetsky [h,i], Stefano Caruso [d], Leonid V. Danyushevky [h], Will Powell [j,k], William L. Griffin [j]

[a] Goethe Universität, Facheinheit Mineralogie, Altenhöferallee 1, 60438 Frankfurt, Germany
[b] Institute of Geochemistry and Petrology, Department of Earth Sciences, ETH, Zurich, Switzerland
[c] Kimberlites and Diamonds (KiDs), School of Earth Sciences, The University of Melbourne, Australia
[d] Centre for Exploration Targeting, School of Earth Sciences, ARC Centre of Excellence for Core to Crust Fluid Systems, University of Western Australia, Australia
[e] School of Biological, Earth and Environmental Sciences, Australian Centre for Astrobiology, PANGEA Research Centre, University of New South Wales, Australia
[f] CSIRO Mineral Resources, Kensington, Australia
[g] LabMaTer (Sciences de La Terre), Université Du Quebec à Chicoutimi, Canada
[h] School of Natural Sciences and Centre of Excellence in Ore Deposits (CODES), University of Tasmania, Australia
[i] Institute of Experimental Mineralogy, Chernogolovka, Russia
[j] Australian Research Council Centre of Excellence for Core to Crust Fluid Systems (CCFS)/GEMOC, Department of Earth and Planetary Sciences, Macquarie University, Australia
[k] Rio Tinto Exploration, Bundoora, Australia

ARTICLE INFO

Article history:
Received 15 April 2020
Received in revised form 2 November 2020
Accepted 10 November 2020
Available online 13 November 2020

Keywords:
Platinum-group elements
Highly siderophile elements
Alloy
Base metal sulphides
Cratonic lithosphere
Metasomatism

ABSTRACT

The metasomatised continental mantle may play a key role in the generation of some ore deposits, in particular mineral systems enriched in platinum-group elements (PGE) and Au. The cratonic lithosphere is the longest-lived potential source for these elements, but the processes that facilitate their pre-concentration in the mantle and their later remobilisation to the crust are not yet well-established. Here, we report new results on the petrography, major-element, and siderophile- and chalcophile-element composition of native Ni, base metal sulphides (BMS), and spinels in a suite of well-characterised, highly metasomatised and weakly serpentinised peridotite xenoliths from the Bultfontein kimberlite in the Kaapvaal Craton, and integrate these data with published analyses. Pentlandite in polymict breccias (failed kimberlite intrusions at mantle depth) has lower trace-element contents (e.g., median total PGE 0.72 ppm) than pentlandite in phlogopite peridotites and Mica-Amphibole-Rutile-Ilmenite-Diopside (MARID) rocks (median 1.6 ppm). Spinel is an insignificant host for all elements except Zn, and BMS and native Ni account for typically <25% of the bulk-rock PGE and Au. High bulk-rock Te/S suggest a role for PGE-bearing tellurides, which, along with other compounds of metasomatic origin, may host the missing As, Ag, Cd, Sb, Te and, in part, Bi that are unaccounted for by the main assemblage.

The close spatial relationship between BMS and metasomatic minerals (e.g., phlogopite, ilmenite) indicates that the lithospheric mantle beneath Bultfontein was resulphidised by metasomatism after initial melt depletion during stabilisation of the cratonic lithosphere. Newly-formed BMS are markedly PGE-poor, as total PGE contents are <4.2 ppm in pentlandite from seven samples, compared to >26 ppm in BMS in other peridotite xenoliths from the Kaapvaal craton. This represents a strong dilution of the original PGE abundances at the mineral scale, perhaps starting from precursor PGE alloy and small volumes of residual BMS. The latter may have been the precursor to native Ni, which occurs in an unusual Ni-enriched zone in a harzburgite and displays strongly variable, but overall high PGE abundances (up to 81 ppm). In strongly metasomatised peridotites, Au is enriched relative to Pd, and was probably added along with S. A combination of net introduction of S, Au +/− PGE from the asthenosphere and intra-lithospheric redistribution, in part sourced from subducted materials, during metasomatic events may have led to sulphide precipitation at ~80–120 km beneath Bultfontein. This process locally enhanced the metallogenic fertility of this lithospheric reservoir. Further mobilisation of the metal budget stored in these S-rich domains

* Corresponding author at: Institute of Geochemistry and Petrology, Department of Earth Sciences, ETH, Zurich, Switzerland.
** Corresponding author at: Goethe Universität, Facheinheit Mineralogie, Altenhöferallee 1, 60438 Frankfurt, Germany.
E-mail addresses: s.aulbach@em.uni-frankfurt.de (S. Aulbach), andrea.giuliani@erdw.ethz.ch (A. Giuliani).

https://doi.org/10.1016/j.lithos.2020.105880

and upwards transport into the crust may require interaction with sulphide-undersaturated melts that can dissolve sulphides along with the metals they store.

1. Introduction

Due to its longevity, ancient (cratonic) continental lithosphere is not only the sole archive of Earth's early compositional and dynamic evolution, but it is also host to economically important diamond, PGE and Au ore deposits (e.g., De Wit and Thiart, 2005; Groves et al., 1987; Hawkesworth et al., 2017). The metasomatised lithospheric mantle, in particular that affected by subduction processes, has been implicated in the generation of some of these, by yielding or contributing to magmas that ascended and mineralised shallower levels of the lithosphere (e.g., Griffin et al., 2013; Rielli et al., 2018a, 2018b; Holwell et al., 2019; Wang et al., 2020). On the other hand, a role for the continental mantle as a source of precious and base metals has been questioned by some authors (e.g., Arndt, 2013; Maier et al., 2017), warranting further work on the main processes responsible for the concentration of siderophile elements in, and their remobilisation from, the lithospheric mantle.

In the absence of a metal phase, PGE may be sequestered into sulphides (e.g., Lorand et al., 2008, 2010; Lorand and Alard, 2010; Luguet et al., 2004; Pattou et al., 1996). Combined with evidence for the depth of metal saturation in the Earth's mantle at ~250 km (Ballhaus, 1995; Rohrbach et al., 2007), which roughly corresponds to the lithosphere-asthenosphere boundary beneath intact cratons, the highly chalcophile and siderophile character of PGE suggests that they should largely reside in sulphide or platinum-group minerals (PGM; e.g., Luguet et al., 2007; Lorand and Luguet, 2016) in the lithospheric mantle.

Magmas and related fluids episodically ascending through the mantle lithosphere are the main agents of its metasomatic modification (e.g., Menzies and Hawkesworth, 1987; O'Reilly and Griffin, 2013; Pearson and Wittig, 2014). Such changes include the stabilisation or destabilisation of metal alloys and sulphides, depending on the mineral saturation or undersaturation state in any given metasomatising melt as a function of pressure, temperature, composition, and f_{O2} (e.g., Chowdhury and Dasgupta, 2020; Mavrogenes and O'Neill, 1999; Mungall and Brenan, 2014; Woodland et al., 2019; Wykes et al., 2015). As a consequence, metasomatism and associated changes in fO_2 also have a strong effect on the metal endowment of the lithosphere, where both subduction-related and asthenospheric fluids and melts are important (e.g., Tassara et al., 2017, 2020; Holwell et al., 2019; Lawley et al., 2020a; Wang et al., 2020; Choi et al., 2020). An association of sulphides with metasomatism in the lithospheric mantle of the Kaapvaal Craton is well established (Aulbach et al., 2009a, 2009b; Burness et al., 2020; Giuliani et al., 2013a, 2013b, 2016a; Lorand and Grégoire, 2006), but the siderophile and chalcophile element composition of sulphides remains poorly known. Moreover, recent work has highlighted that, despite the known link of serpentinised ophiolite complexes with economic placer PGM deposits, details of precious metal remobilisation during hydrothermal alteration remain only partially understood (Savelyev et al., 2018, and references therein; Lawley et al., 2020b). Since kimberlite-hosted mantle xenoliths commonly show features of partial desulphurisation owing to serpentinisation (e.g., Giuliani et al., 2016a; Lorand and Grégoire, 2006), their study may provide important natural analogues for the behaviour of siderophile elements during the onset of serpentinisation.

Here, we targeted one unusual Ni-mineralised and eight highly metasomatised peridotite xenoliths from the ~88 Ma Bultfontein kimberlite in the Kimberley area of the western Kaapvaal Craton. All samples are well-characterised and are only mildly serpentinised (Fitzpayne et al., 2019a, 2020; Giuliani et al., 2013a, 2013b, 2014a, 2014b, 2016a, 2016b; Lawless et al., 1979; Zhang et al., 2000, 2001, 2003). We undertook a detailed major- and trace-element study of their sulphide, native Ni and spinel minerals in order to i) constrain the extent to which the budget of the PGE and other metals is controlled by these phases, and ii) understand the formation and stability of these minerals and the mobility of metals and metalloids (e.g., As, Sb) during metasomatic processes in the mantle and alteration processes after kimberlite emplacement. Ultimately, this study bears on the mechanisms of metal pre-concentration in the continental lithosphere, which may be one first-order control on the localisation and genesis of economically important ore deposits.

2. Geology, samples and prior work

The Kaapvaal Craton consists of two major Archaean terranes: i) the 3.55 to 3.05 Ga Witwatersrand Block in the east; ii) the younger, 3.15 to 2.90 Ga Kimberley Block in the west (de Wit et al., 1992; Fig. 1). The 2.93 to 2.88 Ga Colesberg lineament is interpreted as the surface expression of their collision (Schmitz et al., 2004). The craton was affected by multiple collisional events at its margins, such as the ~2.0 to 1.7 Ga Kheis-Magondi orogeny to the west (Cornell et al., 1998; Griffin et al., 2003), and the 1.10 to 1.05 Ga Kibaran orogeny to the south leading to formation of the Namaqua-Natal fold belt (Jacobs et al., 2008). Major post-Archaean magmatic events include emplacement of the ca. 2.06 Ga giant Bushveld Complex (Buick et al., 2001), and the 185 to 174 Ma Karroo large igneous province (Duncan et al., 1997), followed by >110 Ma lamproite (formerly orangeite, aka Group II kimberlite) and ≤100 Ma kimberlite magmatism (Griffin et al., 2014a; Giuliani et al., 2015, and references therein).

Several different effects of these multiple processes on the deep lithosphere have been recognised. Craton amalgamation with closure of an

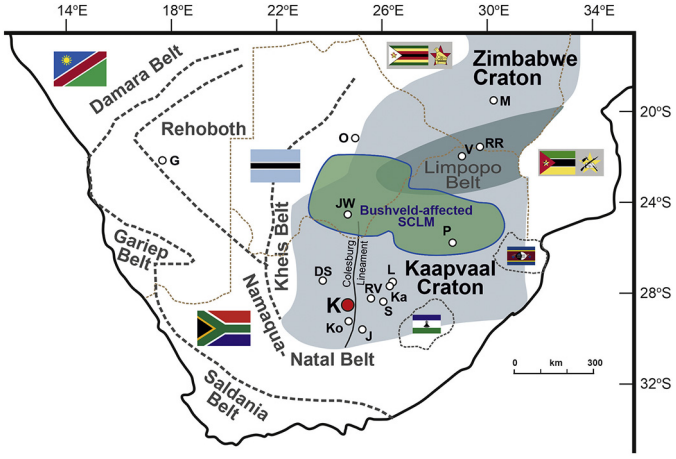

Fig. 1. Map of southern Africa (after Pearson et al., 1998; Shirey et al., 2002) with outline of the Kaapvaal craton, Zimbabwe craton and intervening Limpopo Belt, showing the approximate locations of the Kimberley kimberlites (K) including Bultfontein, and some other kimberlite and lamproite localities (DS Doornkloof-Sover, G Gibeon, J Jagersfontein, JW Jwaneng, L Lace, Ka Kaalvallei, Ko Koffiefontein, M Murowa, O Orapa, P Premier, RR River Ranch, RV Roberts Victor, S Star, V Venetia). The outline of the area with an imprint of the ca 2 Ga Bushveld large igneous event on the subcontinental lithospheric mantle and some Proterozoic mobile belts are shown along with political boundaries (thin stippled lines).

intervening ocean basin at ca. 2.9 Ga led to volatile enrichment (Bell et al., 2005; Peslier et al., 2012), including introduction of recycled subducted components (Eldridge et al., 1991; Thomassot et al., 2009), and emplacement of subducted oceanic crust, now sampled as eclogite xenoliths and eclogitic diamonds (e.g., Jagoutz et al., 1984; Richardson et al., 2001). Proterozoic subduction processes at the craton margins are reflected in renewed diamond growth events (Richardson et al., 1990), accompanied by addition of volatiles, which may have been sourced from deeply subducted crustal lithologies (e.g., Fitzpayne et al., 2019a; Giuliani et al., 2016a). The imprints of large igneous events are reflected in low seismic velocities and diamond growth in a large area around the Bushveld Complex (Shirey et al., 2002; Shirey et al., 2008), and in strongly metasomatised rocks with lindsleyite–mathiasite (LIMA) titanate minerals dated to the age of Karoo magmatism (Giuliani et al., 2014b; Griffin et al., 2014b). Finally, heating, refertilisation, and metasomatism, presumably in relation to plume impingement (Le Roex, 1986), occurred between Jurassic-Cretaceous lamproite and Cretaceous kimberlite magmatism (Bell et al., 2005; Kobussen et al., 2009).

The samples selected for this study were collected from the Boshof Road dumps in Kimberley (South Africa), which host historical waste material from the Bultfontein kimberlite. The Bultfontein pipe is part of the Kimberley cluster of archetypal kimberlites, which also includes the De Beers, Dutoitspan, Wesselton and Kimberley kimberlites, along with a number of smaller pipes. It is located in the southwestern Kaapvaal Craton (Field et al., 2008; Giuliani et al., 2017; Le Roex et al., 2003). The Bultfontein kimberlite was emplaced at 88.3 ± 0.2 Ma based on phlogopite Rb-Sr dating (Fitzpayne et al., 2020), which is in the ~84–92 Ma age range of other Kimberley kimberlites (Griffin et al., 2014a and references therein). The Kimberley kimberlites are well known for hosting a variety of mantle xenoliths showing distinct metasomatic styles, e.g., MARID, PIC (phlogopite-ilmenite-clinopyroxene), polymict breccias, websterites, wehrlites, etc. (Dawson and Smith, 1977; Erlank et al., 1987; Fitzpayne et al., 2018, 2019a, 2019b; Giuliani et al., 2013a, 2014a, 2014b; Grégoire et al., 2002, 2003; Lawless et al., 1979; Rehfeldt et al., 2008; Simon et al., 2007). Salient characteristics of the samples are provided in Table 1, and additional details on their petrogenesis in Appendix 1. For comparative purposes, we also analysed the major- and trace-element compositions of spinel in five spinel lherzolites from Pliocene-Pleistocene alkali basalt volcanoes in southeastern Australia (MSHX-2 and MSHX-3 from Mt Shadwell; BLMX-2, BLMX-4 and BLMX-7 from Bullenmerri).

To examine the trace-element composition of sulphides (plus native Ni, spinels and Ti-oxides) in metasomatised mantle xenoliths from the Kimberley area (Fig. 1), we selected the following samples (Table 1): i) three phlogopite-rich spinel peridotites, which are akin to the PKP (phlogopite–K-richterite peridotites) of Erlank et al. (1987); ii) a phlogopite-free spinel harzburgite containing native Ni and sulphides

Table 1
Petrographic and geochemical features and age constraints for studied mantle xenoliths from the Bultfontein kimberlite.

Sample name	Lithology	Texture	Main minerals (≥ 5 vol.%)	Minor minerals (<5 vol.%)	Sulphide minerals[1]	Sulphide $\delta^{34}S$ (‰)	Olivine Mg# (±1σ)	Phlogopite TiO_2 (wt.%, ±1σ)	Equilibrium T (°C)[2]	Equilibrium P (GPa)[3]	Age of metasomatism (Ma)	References
DU-1	polymict breccia	porphyroblastic	(Ol, Opx, Phl, Ilm, Rt)[a]	Sulf	Pn, Cp, Po	−1.0 to −5.4	88.4 ± 0.4	3.61 ± 0.28	850–900	3.4–3.7	~80–90[b]	A, B, C, D
BD2666	polymict breccia	porphyroblastic	(Ol, Opx, Phl, Ilm, Rt)[a]	Sulf	Pn, Cp, Po						~83[c]	E, F, G, H, I
JJG1414	polymict breccia	porphyroblastic	(Ol, Phl, Ilm, Rt)[a]	Sulf	Pn, Cp, Po						~80–90[b]	E, F, G, H, I
JJG513	polymict breccia	porphyroblastic	(Ol, Opx, Phl, Ilm, Rt)[a]	Sulf	Pn, Cp, Po						~80–90[b]	E, F, G, H, I
XM1/142	Phl-rich Spl harzburgite (PKP)	coarse-granular	Ol, Opx, Phl	Cpx, Kric, Spl, Sulf	Pn	−2.1 to −5.3	92.3 ± 0.2	0.64 ± 0.02	750–860	3.0–3.5	82 ± 3[d]	D, J, K, L, M
XM1/341	Phl-rich Spl lherzolite (PKP)	granular	Ol, Opx, Cpx, Phl	LIMA, Spl, Sulf	Pn	−5.4	89.7 ± 0.2	0.76 ± 0.03	830–910	3.4–3.8	177 ± 12[e]	D, K, L, M, N, O
XM1/345	Phl-rich Spl harzburgite (PKP)	granular	Ol, Opx, Phl	Cpx, LIMA, Spl, Ilm, Sulf	Pn	−2.6 to −5.9	89.2 ± 0.1	0.78 ± 0.04	750–850	3.0–3.4	178 ± 29[e]	D, K, M, N, O
XM1/422	Spl harzburgite	coarse-granular	Ol, Opx	Spl, Cpx, Sulf, native Ni	Hz*, Djerf		92.6 ± 0.1		670–720	2.6–2.8	~80–90[f]	P
BLFX-3	MARID	foliated	Phl, Kric	Cpx, Ilm, Sulf	Pn			0.27 ± 0.01			no constraints	

A: Giuliani et al., 2012; B: Giuliani et al., 2013b; C: Giuliani et al., 2014a; D: Giuliani et al., 2016a; E: Lawless et al., 1979; F: Wyatt and Lawless, 1984; G: Zhang et al., 2000; H: Zhang et al., 2001; I: Zhang et al., 2003; J; Konzett et al., 2000; K: Fitzpayne et al., 2019a; L: Fitzpayne et al., 2019b, submitted to Lithos; M: Giuliani et al., 2016b; N: Giuliani et al., 2014b; O: Giuliani et al., 2018; P: Giuliani et al., 2013a.

Ol: olivine, Opx, orthopyroxene, Cpx: clinopyroxene; Phl: phlogopite; Kric: K-richterite; Spl: spinel; Ilm: ilmenite; Rt: rutile; LIMA: lindleyite-mathiasite group; Sulf: sulfides; Pn: pentlandite; Cp: chalcopyrite; Po: pyrrhotite; Hz: heazlewoodite; Djerf: djerfisherite.

[1] Alteration phases include heazlewoodite after pentlandite, digenite after chalcopyrite; * large hz grains contain 5 micron inclusions of native Cu, Cu-sulphide and Sb-bearing gersdorffite (NiAsS).

[2] Temperature calculated using thermometers based on the following equilibria: orthopyroxene-clinopyroxene solvus (Taylor, 1998; Wells, 1977), Ca in orthopyroxene (Brey et al., 1990), Fe-Mg exchange between olivine and spinel (Ballhaus et al., 1991).

[3] Pressure calculated using T values and assuming equilibrium along a 40 mW/m^2 geotherm, which is appropriate for the lithospheric mantle beneath Kimberley (Bell et al., 2004).

[a] Magmatic groundmass; the sample hosts abundant porphyroclasts of olivine, garnet, orthopyroxene, clinopyroxene and phlogopite.

[b] Metasomatism coeval with kimberlite magmatism in the Kimberley area (Giuliani et al., 2014a; Lawless et al., 1979; Zhang et al., 2000).

[c] Zircon U/Pb age (Lawless et al., 1979).

[d] Zircon U/Pb age (Konzett et al., 2000).

[e] LIMA U/Pb age (Giuliani et al., 2014b).

[f] Metasomatism coeval with kimberlite magmatism in the Kimberley area (Giuliani et al., 2013a).

(Giuliani et al., 2013a); iii) a MARID rock; iv) four mantle polymict breccias, which represent mixtures of mantle-derived grains cemented by metasomatic phases. Polymict breccias are commonly interpreted as aborted kimberlite intrusions at mantle depths (e.g., Giuliani et al., 2014a; Lawless et al., 1979), which provide information on lithospheric enrichment processes in relation to kimberlite magmatism. Sample selection was based on two criteria: samples exhibiting different metasomatic styles; and availability, size and alteration conditions of sulphide minerals and native Ni.

3. Native Ni, sulphide and oxide petrography

3.1. Nickel-rich spinel harzburgite (Ni-harzburgite)

Sample XM1/422 is a coarse-grained, granular spinel harzburgite that contains symplectites of spinel + clinopyroxene + orthopyroxene, which are locally overprinted by Ni-rich phases (Fig. 2A,D; Giuliani et al., 2013a). These include a Ni-dominated alloy (i.e. native Ni) with variable Fe contents (up to ~13 wt%), heazlewoodite [Ni_3S_2], Ni-Fe-rich olivine, Ni-Fe-rich clinopyroxene, Ni-Fe-rich spinel and Ni-rich phlogopite, associated with minor apatite, aegirine, djerfisherite [$K_6Na(Fe,Cu,Ni)_{25}S_{26}Cl$], as well as carbonates and halides (Fig. 2). Spinel occurs as discrete grains with equant or vermicular shape (Fig. 2A,F; Fig. 3C) and in symplectites (see Giuliani et al., 2013a for representative images). The heazlewoodite in this xenolith is not an alteration phase, but rather represents the low-T polymorph of $\alpha Ni_{3\pm x}S_2$, which is stable up to 862 °C (Karup-Møller and Makovicky, 1995). One heazlewoodite inclusion in olivine hosts a sub-micrometric Pt-Au alloy inclusion (Fig. 2H,I). Similar native Ni-heazlewoodite associations were reported from other mantle xenoliths from Bultfontein and nearby Jagersfontein (Lorand and Grégoire, 2006).

3.2. Phlogopite-rich spinel peridotites (phl-peridotites)

This group comprises a coarse-grained, granular phlogopite-rich spinel harzburgite with minor clinopyroxene and K-richterite (sample XM1/142), a moderately coarse-grained, LIMA-bearing, phlogopite-rich spinel lherzolite (XM1/341), and a coarse-grained spinel harzburgite (XM1/345) with phlogopite-rich bands containing clinopyroxene, ilmenite and LIMA (Giuliani et al., 2014b, 2016a, 2016b, 2018). In sample XM1/142, pentlandite is closely associated with other metasomatic phases, i.e. clinopyroxene and phlogopite, and

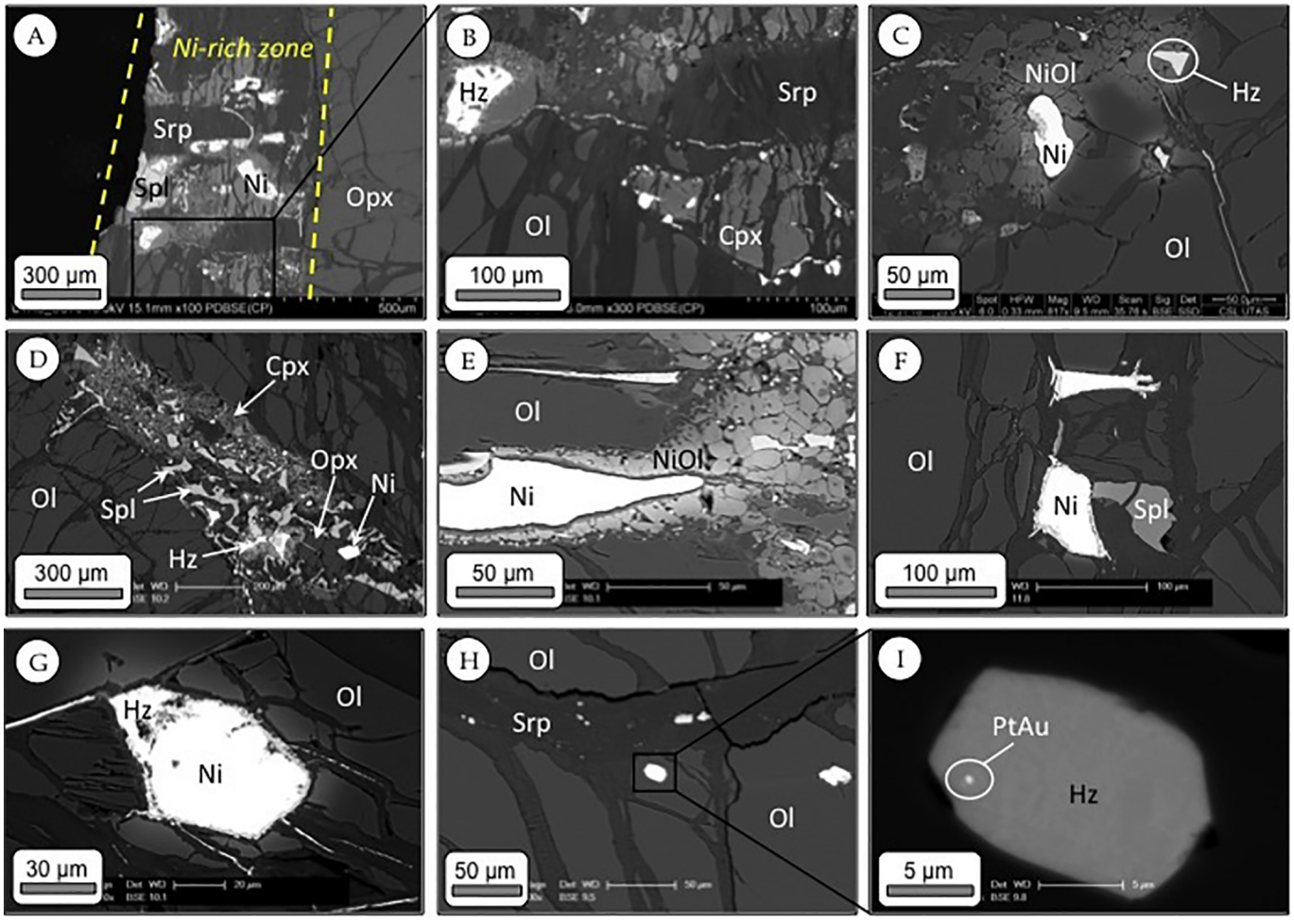

Fig. 2. Scanning-electron microscope (SEM) back-scattered electron (BSE) images of sulphides and native Ni in Ni-enriched harzburgite sample XM1/422. (A-B) Ni-rich zone with native Ni (Ni), heazlewoodite (Hz), abundant spinel (Spl) and clinopyroxene (Cpx); in b) the bright veinlets and small grains encircling clinopyroxene are heazlewoodite. (C) Ni-rich zone with native Ni and heazlewoodite; note the brighter tinge of olivine in contact with the Ni-rich phases due to diffusive enrichment of Ni and Fe into olivine (NiOl). (D) Symplectite of spinel + orthopyroxene (Opx) + clinopyroxene overprinted by the Ni-rich assemblage, including native Ni and heazlewoodite. (E) Another example of a Ni-enriched assemblage where native Ni is associated with abundant neoblastic Ni-rich olivine (NiOl). (F) Example of the common association between native Ni and spinel in this sample. (G) Overgrowth of heazlewoodite on native Ni; note the bright halo surrounding the Ni-rich phases due to Ni and Fe diffusion into adjacent olivine, and the occurrence of late-stage bright heazlewoodite veinlets associated with serpentine. (H-I) Heazlewoodite inclusion in olivine nearby a serpentine (Srp)-filled fracture, which hosts a sub-micrometric inclusion of Pt-Au alloy. The images in panels (D) and (G) have been modified from Giuliani et al. (2013a).

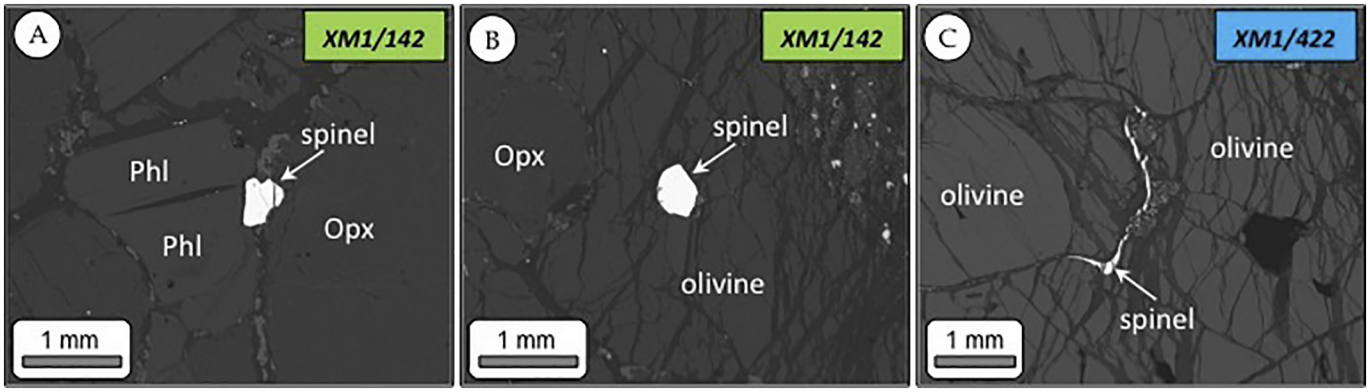

Fig. 3. SEM BSE images of typical petrographic occurrences of spinel in the examined samples: (A) Spinel associated with metasomatic phases – phlogopite (Phl) and orthopyroxene (Opx), phl-peridotite sample XM1/142. (B) Spinel included in olivine in sample XM1/142. (C) Vermicular spinel in Ni-enriched peridotite XM1/422.

also occurs included in orthopyroxene (Giuliani et al., 2016b). Pentlandite grains (up to ~500 μm across) show compositional variations between Ni-rich and Fe-rich domains (Fig. 4G–I) and are typically fractured, with serpentine and small (up to 20–25 μm) magnetite segregations filling up the interstitial spaces. Alteration to heazlewoodite ± magnetite is sparse (<10% of observed areas). Pentlandite in this and

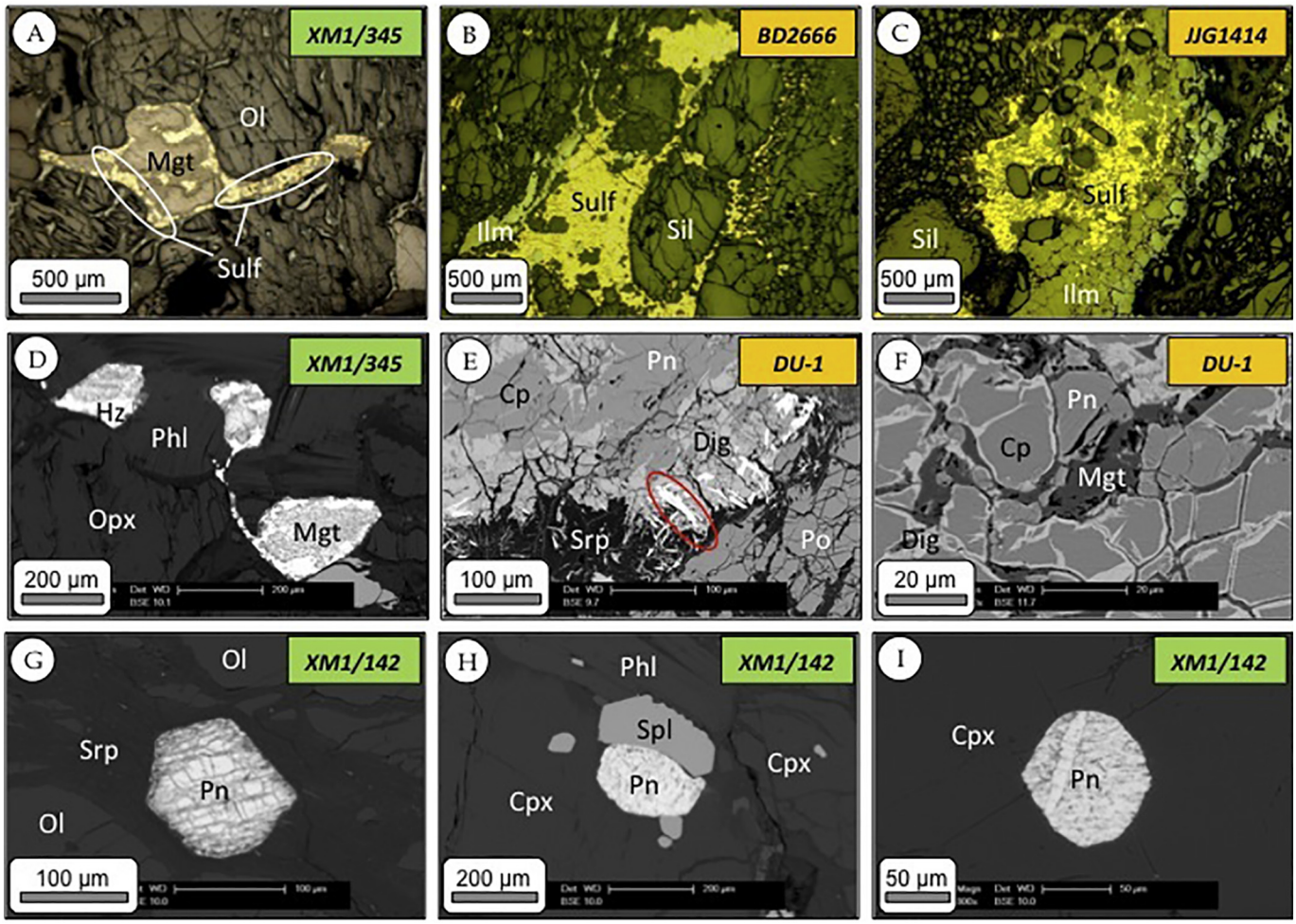

Fig. 4. Optical micro-photographs (A–C) and SEM BSE images (D–I) of sulphide minerals in phlogopite-rich peridotites and mantle polymict breccias. (A) Interstitial sulphide (Sulf) aggregate (pentlandite and secondary heazlewoodite) largely replaced by magnetite (Mgt) in phl-peridotite sample XM1/345. (B–C) Large interstitial segregations of sulphides in polymict breccias; note the typical association of sulphides with ilmenite (Ilm) in these samples. (D) Sulphides grains altered to magnetite and heazlewoodite (Hz) and texturally associated with phlogopite (Phl) and orthopyroxene (Opx) in phl-peridotite sample XM1/345. (E–F) Details of sulphide segregations in polymict breccias consisting of pentlandite (Pn), chalcopyrite (Cp), less common pyrrhotite (Po) and their alteration products – e.g., digenite (Dig), an unidentified Cu-Fe sulfide (red oval), heazlewoodite (not indicated), and magnetite with interstitial serpentine (Srp). (G–I) Fresh pentlandite grains in phl-peridotite sample XM1/142 located along grain boundaries between olivine (G), texturally associated with clinopyroxene (Cpx) and spinel (Spl, panel (H), or included in clinopyroxene (I). Ol: olivine; Sil: silicate minerals.

the other mantle xenoliths described below is a low-T phase (<600°C) derived from re-equilibration of monosulphide solid solution (mss) ± $\alpha Ni_{3\pm x}S_2$ to pentlandite + pyrrhotite, where pyrrhotite was replaced by magnetite during serpentinisation (Giuliani et al., 2016b). Typical spinel grains show equant shapes (Fig. 3A,B). Compared to sample XM1/142, pentlandite grains in XM1/341 are fresh (i.e. minor replacement by heazlewoodite ± magnetite) only where included in clinopyroxene and, occasionally, phlogopite. The inclusions are smaller (20–60 μm) than the entirely altered interstitial grains (up to 300 μm). In sample XM1/345, sulphides are located in the phlogopite-rich bands and form large (up to ~1 mm) interstitial segregations, which are almost completely altered to magnetite and heazlewoodite with only minor fresh pentlandite (Giuliani et al., 2016b; Fig. 4A,D). Abundant (former) pentlandite inclusions occur in partially serpentinised orthopyroxene, but were largely replaced by heazlewoodite and magnetite.

3.3. MARID

Sample BLFX-3 has a foliated texture and consists of alternating bands enriched in either phlogopite or K-richterite. Ilmenite is common in both phlogopite-rich and amphibole-rich layers, whereas clinopyroxene and rutile are absent. Rare pentlandite (<60 μm) occurs included in K-richterite. Alteration of pentlandite to heazlewoodite and magnetite is common. Other minor base-metal sulphides (BMS) (<10–20 μm) occur in secondary calcite-rich veins with diopside and minor barite and pectolite.

3.4. Polymict breccias

Mantle polymict breccias (or peridotites) consist of mixtures of mantle-derived clasts (mainly olivine, garnet, clinopyroxene and orthopyroxene) of variable composition and origin (e.g., garnets of peridotitic, eclogitic, pyroxenitic, websteritic and megacrystic paragenesis; Zhang et al., 2003). These phases are set in a relatively fine-grained matrix of olivine, phlogopite, ilmenite and rutile, with variable and locally abundant orthopyroxene and minor sulphides (Giuliani et al., 2014a; Lawless et al., 1979). The other prominent feature of these xenoliths is the presence of large lenses and veins of ilmenite + rutile (Giuliani et al., 2012, 2013b; Wyatt and Lawless, 1984; Zhang et al., 2001), which locally are associated with large (up to 2.0×0.5 cm) segregations of BMS (Giuliani et al., 2013b, 2016b). The fresh parts of these segregations are composed of intergrown pentlandite, chalcopyrite, and rare pyrrhotite with secondary Cu- and Ni-sulphides (i.e. digenite, chalcocite and heazlewoodite; Fig. 4B,C,E,F). Sulphide segregations are usually replaced by magnetite (±hematite as a supergene alteration product) with lesser Cu sulphides, Ni sulphides and native Cu, presumably in relation to low-T serpentinisation, as also observed by Lorand and Grégoire (2006) on a separate xenolith suite from Bultfontein and nearby kimberlites.

4. Sample preparation and analytical techniques

The petrography of sulphide minerals was undertaken at the University of Melbourne, using a petrographic microscope and a Philips (FEI) XL30 Environmental Scanning Electron Microscope (ESEM), equipped with an Oxford INCA Energy-Dispersive X-ray Spectrometer (EDS). A Cameca SX50 Electron Microprobe was used for quantitative analysis of major- and minor-element compositions (Giuliani et al., 2016a). Details on the methods and results are given in Appendices 1 and 2, respectively. Trace-element concentrations in sulphides were acquired *in situ* by laser ablation microprobe inductively-coupled mass spectrometry (LAM-ICPMS) at CODES, University of Tasmania, where a RESOlution 193 nm excimer laser microprobe coupled to an Agilent 7700 quadrupole mass-spectrometer was employed (Gilbert et al., 2013), and at Macquarie University, using an Agilent 7700 ICP-MS coupled to a Photon Machines 193 nm Analyte Excite laser ablation system following protocols outlined at http://gemoc.mq.edu.au/AnMethods/AnlyticalMeth.html#3.2. Details of the data reduction are given in Appendix 1, and results with typical limits of detection (LOD) are reported in Appendix 3. The analysis by LAM-ICPMS of mantle sulphides, which are affected by the presence of inclusions, low-temperature re-equilibration and serpentinisation, presents specific challenges that are reviewed in Appendix 1, along with information on how these were dealt with in this study.

Spinel was analysed for major elements using a JEOL 8530F field-emission gun electron probe micro-analyser at the Centre for Microscopy, Characterisation and Analysis of the University of Western Australia (CMCA-UWA). Additional data were collected at the University of Melbourne using equipment and protocols described by Giuliani et al. (2013a; Appendix 4). Quantitative X-ray maps were acquired using the calibration setup described in Appendix 1. Trace-element concentrations were determined *in situ* by LAM-ICPMS at Université du Québec à Chicoutimi (LabMaTer) following methods outlined by Pagé et al. (2012) and Arguin et al. (2016), employing a RESOlution S-155 Excimer laser ablation microprobe (193 nm, Applied Spectra) coupled with an Agilent 7900 Series. Further details are given in Appendix 1, and results in Appendix 5.

5. Results

5.1. Sulphide major elements

The major-element compositions of native Ni and sulphide phases in most of the samples in this study were characterised previously (Giuliani et al., 2013a, 2013b, 2016b; see also Table 1 for mineral assemblages in each sample). New analyses are reported for sulphide minerals in the mantle polymict breccias (except sample DU-1), which include pentlandite, chalcopyrite, pyrrhotite, as well as their alteration products. Whereas analysed pentlandite in three of these samples has uniform average (Fe+Co+Ni+Cu)/S (metal/S atomic) of 1.15 to 1.16, their Ni, Fe and Co contents vary from 29.5 to 36.8 wt%, 29.2 to 35.9 wt%, and 0.75 to 0.93 wt%, respectively (Appendix 2). Chalcopyrite in two samples shows significant variation with respect to Ni (0.69 and 6.6 wt%) and Cu (27.0 and 33.4 wt%), which may relate to co-ablation of pentlandite inclusions beneath the surface. A single analysis of pyrrhotite shows detectable Ni contents (1.06 wt%). The only analysed heazlewoodite grain contains 0.92 wt% Fe, 0.24 wt% Co and 0.44 wt% Cu (Appendix 2). Detected O contents in all minerals are <0.6 wt%, except 0.82 wt% in chalcopyrite from BD2666.

5.2. Sulphide trace elements

The trace elements in native Ni and sulphide phases described in this section are free of detectable inclusions and grain-boundary contamination, although we cannot exclude the presence of micro- or nano-nuggets too small to be resolved by LAM-ICPMS (Appendix 1). Because altered mixed sulphides (containing fine intergrowths of magnetite or heazlewoodite related to serpentinisation) and analyses of sulphides with >40,000 ppm Si were filtered out, no analyses are described for sample XM1/341. Some samples show strong trace-element variations in their sulphides (Fig. 5), with large standard deviations for multiple spots per grain (Table 2). Median abundances were calculated to mitigate the effects of outliers. Note that Zn, Ga, Mo, Sb and Re are semi-quantitative values because the calculated medians include analyses that were calibrated against silicate glass, which can generate considerable errors (Appendix 1).

Native Ni in peridotite sample XM1/422 contains up to several ppm of the IPGE (Ir-group PGE: Os, Ir, Ru), commonly <0.5 ppm of the PPGE (Pt-group PGE: Rh, Pt, Pd), and <0.05 ppm Re and Au, although concentrations vary widely (Table 2). It further contains 3100 ppm Co, 3300 ppm Cu and 19.3 ppm Zn. Abundances of As, Mo and Pb are

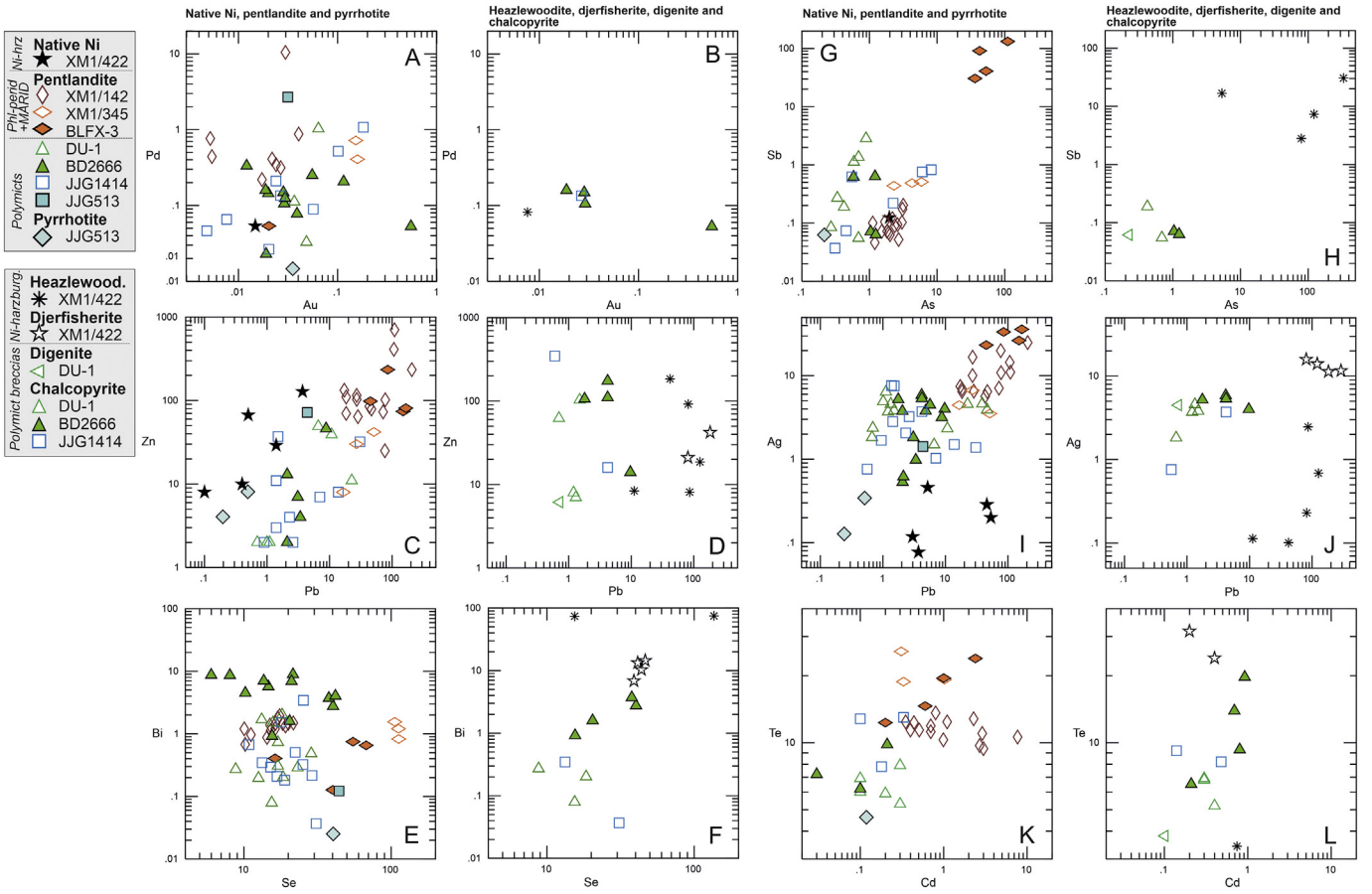

Fig. 5. Trace element-abundances (ppm) in native Ni and sulphides in Ni-enriched harzburgite (Ni-hrz, Ni-harzb), phlogopite-rich peridotites (Phl-perid), MARID and polymict breccia (Polymicts) xenoliths from Bultfontein. Heazlewoodite (Heazlewood.), djerfisherite, digenite and chalcopyrite are shown in separate panels next to native Ni, pentlandite and pyrrhotite for clarity. All individual analyses are shown to illustrate trace-element variability.

<10 ppm, varying by several orders of magnitude for Mo and Pb. Concentrations of Ag, Cd and Sb are <1 ppm and of Bi <0.1 ppm (mostly <LOD), whereas Se and Te are generally <LOD. The co-existing djerfisherite has PGE abundances <0.2 ppm, with similar Re (0.037 ppm) and undetectable Au. It further has somewhat higher median Co, Cu and Zn abundances (median 6100, 5700 and 32 ppm, respectively), as well as markedly higher abundances of chalcophile elements (43 ppm Se, 38 ppm Mo, 12 ppm Ag, 0.3 ppm Cd, 28 ppm Te, 152 ppm Pb, 11.8 ppm Bi; n = 4) (Table 2). All but one analysis of the primary heazlewoodite display Re and Au <LOD, and median PGE abundances <0.3 ppm, except for Os with 2.7 and Ir with 1.46 ppm, although large variations are observed (Table 2). It shows highly variable compositions with respect to the remaining elements: Co 440–9400 ppm, Cu 112–2800 ppm, Zn 8–185 ppm, As 5.3–330 ppm, Se up to 136 ppm (3 out of 5 analyses <LOD), Mo 0.25–7.0 ppm, Ag 0.10–2.5 ppm, Cd 0.18–8.7 ppm, Sb 0.80–30.5 ppm, Te 0.11–30 ppm, Pb 11.2–126 ppm, and Bi 0.11–75 ppm (n = 5).

Pentlandite analyses are available for seven of the samples. Highly siderophile element (HSE)-abundances are variable, and, with the exception of pentlandite in polymict breccia JJG513, tend to be higher in the phl-peridotites than in the polymict breccias (Table 2). Pentlandite has median Co, Cu and Zn contents of 2500–18100 ppm, 1830–18900 ppm and 5.8–103 ppm, respectively (Fig. 5; Table 2). Abundances of Se (median 18.9 ppm), Mo (10.2 ppm), Cd (0.28 ppm) and Te (7.0 ppm) vary by less than a factor of 10 between samples, yet larger ranges are observed for As (0.40–48 ppm), Ag (1.4–30 ppm), Sb (0.031–66 ppm), Pb (2.3–118 ppm) and Bi (0.12–6.3 ppm). Large standard deviations for the latter elements in some samples reflect within-sample heterogeneity (Table 2). Higher abundances of Pb, Zn, Ag, Cd and Te are observed in phl-peridotites and MARID than in polymict breccias, with As, Sb, Ag and Pb being higher in the MARID pentlandite (Fig. 5). Pyrrhotite in one of the polymict breccias (JJG513; n = 2) has low contents of the PPGE (0.056 ppm Rh, Pt <LOD, 0.015 ppm Pd), but higher IPGE (0.23 ppm Os, 0.25 ppm Ir, 0.32 ppm Ru) and Re contents (0.11 ppm) (Table 2; Fig. 5). Abundances of Zn (6 ppm) and Pb (0.38 ppm) are also low.

The concentrations of Re (0.020–0.033 ppm), Ir (0.015–0.028 ppm and Ru (0.110–0.115 ppm) in chalcopyrite in three polymict breccias are similar (Fig. 5), with Os in only one sample >LOD (0.028 ppm) and Ru always <LOD. In contrast, Pt and Pd are more variable (0.044–0.31 ppm and 0.025–0.135 ppm, respectively; Appendix 3). With the exception of Co, Sb, Bi and Pb, the trace element concentrations of other trace elements also vary little (Fig. 5). Compared to heazlewoodite in the Ni-harzburgite, alteration-related heazlewoodite in polymict breccias has consistently higher Cu (7x), Ag (18x), Te (2x), Re (1.6x), Pd (4x) and Au abundances (9x), but lower Cd (5x), Se (4x) and much lower As (>100x), Os (>100x) and Ir (>60x) (Fig. 5; Table 2). Finally, a single analysis of digenite formed after chalcopyrite in polymict breccia DU-1 shows 0.008–0.083 ppm of the PGE except for Os, which is <LOD, with 3.4–7.5 ppm of Zn, Se, Mo, Ag, and sub-ppm concentrations of As, Sb, Pb and Bi.

5.3. Spinel major elements

In the Ni-harzburgite XM1-422, spinel occurs in various settings including Ni-poor symplectites with orthopyroxene and clinopyroxene, and Ni-enriched relict grains in Ni-mineralised symplectites (Fig. 2; Giuliani et al., 2013a). The symplectitic variety is Al-chromite with low

Table 2
Trace-element (ppm) concentrations in native Ni and sulphides in peridotite xenoliths from Bultfontein.

Mineral	*Mn*	*Ga*	Co	Cu	*Zn*	As	Se	*Mo*	Ag	Cd	*Sb*	Te	Pb	Bi
Ni-mineralised harzburgite XM1/422														
Native Ni (10)	*<LOD*	*10.7*	3121	3346	*19.3*	3.6	<LOD	*2.9*	0.20	0.59	*0.57*	<LOD	3.0	0.040
rsd		*40*	42	39	*252*	41		*440*	76	86	*71*		706	60
min		*3.4*	2185	2961	*4.0*	1.97		*0.100*	0.077	0.39	*0.124*		0.141	0.016
max		*14.9*	5289	6097	*128*	5.3		*29*	0.46	1.48	*0.93*		53	0.066
Hz (5)	*112*	*53*	1974	708	*18.7*	101	76	*3.6*	0.23	0.892	*7.3*	3.4	82	37
rsd	*766*	*140*	205	171	*411*	140	113	*132*	435	453	*167*	485	54	115
min	*75*	*0.58*	440	112	*8.2*	5.3	15.4	*0.25*	0.101	0.178	*0.82*	0.108	11.2	0.107
max	*1585*	*105*	9409	2794	*185*	334	136	*7.0*	2.5	8.7	*30*	30	126	75
Dj (4)	*209*	*0.88*	6147	5661	*32*	1.56	43	*38*	12.8	0.300	*((0.57))*	28	152	11.8
rsd	*55*	*1*	10	69	*46*	3	8	*79*	17	66		21	60	29
min	*127*	*0.87*	5697	2916	*21*	1.53	39	*16.8*	11.3	0.161		23	81	6.8
max	*290*	*0.89*	6597	12057	*42*	1.59	47	*60*	15.9	0.440		35	290	14.5
Phl-rich peridotite XM1/142														
Pn (14)	*201*	*0.064*	2548	4700	*103*	2.1	16.3	*11.0*	8.7	0.88	*0.092*	11.4	45	1.36
rsd	*54*	*197*	12	81	*177*	32	22	*77*	68	225	*48*	10	117	25
min	*88*	*0.029*	2272	2421	*25*	1.12	10.1	*3.5*	5.7	0.35	*0.046*	9.4	17.2	0.68
max	*472*	*0.48*	3474	17196	*704*	3.2	22	*32*	25	7.7	*0.20*	13.6	207	1.95
Phl-rich peridotite XM1/345														
Pn (3)	*60*	*((0.100))*	7939	18891	*30*	4.3	112	*10.2*	4.4	0.33	*0.49*	19	27	1.20
rsd	*177*		23	35	*58*	42	3	*49*	37	123	*7*	20	66	30
min	*54*		5195	18883	*8*	2.3	106	*6.0*	3.5	0.307	*0.44*	18.8	16.6	0.83
max	*241*		8636	30449	*42*	5.9	113	*15.8*	6.7	1.020	*0.51*	26	51	1.55
MARID BLFX-3														
Pn (4)	*36*	*125*	18083	1830	*89*	48	48	*10.685*	30	0.800	*66*	17.0	118	0.530
rsd	*124*	*89*	10	66	*85*	71	46	*93*	20	116	*71*	30	48	52
min	*10*	*15*	15850	574	*74*	36	16.3	*3.7*	23	0.240	*31*	12.3	45	0.127
max	*105*	*261*	19802	2807	*234*	111	68	*26*	36	2.4	*132*	24	166	0.75
Polymict peridotite DU-1														
Pn (6)	*45*	*0.118*	3164	12398	*6.24*	0.41	17.0	*5.6*	3.5	0.236	*0.177*	5.9	3.9	0.39
rsd	*38*	*224*	16	53	*342*	45	36	*43*	55	41	*349*	16	222	142
min	*27*	*0.009*	2619	2196	*1.52*	0.27	12.6	*3.6*	1.49	0.084	*0.053*	5.3	0.69	0.196
max	*76*	*0.68*	3909	19644	*49*	0.69	29	*10.0*	6.4	0.30	*1.36*	7.9	23	1.69
Hz (2)	*61*	*1.61*	1327	4366	*51*	0.74	17.0	*8.2*	4.3	0.186	*1.98*	6.4	43	1.76
rsd	*80*	*80*	30	3	*9*	29	10	*14*	12	22	*62*	9	13	21
min	*26*	*0.69*	1043	4262	*48*	0.59	15.8	*7.4*	3.9	0.156	*1.12*	6.0	39	1.50
max	*96*	*2.5*	1611	4470	*55*	0.89	18.2	*9.1*	4.6	0.22	*2.8*	6.8	46	2.0
Cp (4)	*40*	*0.35*	84	242020	*35*	0.57	15.5	*7.3*	3.8	0.31	*0.060*	6.5	1.28	0.24
rsd	*12*	*130*	94	15	*133*	24	32	*144*	31	11	*127*	12	28	46
min	*36*	*0.028*	23	192284	*6.6*	0.42	8.8	*6.0*	1.82	0.31	*0.055*	5.2	0.67	0.079
max	*48*	*0.68*	210	282644	*103*	0.69	18.5	*28*	4.6	0.37	*0.189*	6.9	1.51	0.33
Dg (1)	*44*	*0.04*	75	307313	*5.5*	0.2	3.4	*7.5*	4.5	0.106	*0.06*	3.8	0.7	0.180
Polymict peridotite BD2666														
Pn (6)	*66*	*0.179*	3972	4598	*5.8*	0.79	11.9	*3.8*	1.40	0.103	*((0.031))*	6.5	2.6	6.3
rsd	*71*	*140*	22	492	*297*	219	110	*49*	98	86		26	100	32
min	*7.5*	*0.099*	2807	671	*2*	0.30	6.0	*2.9*	0.53	0.034		4.7	2.1	4.0
max	*111*	*0.76*	5276	59126	*46*	3.5	42	*7.9*	3.8	0.21		9.8	8.8	8.7
Cp (4)	*66*	*0.085*	537	193876	*108*	1.14	29	*7.0*	5.3	0.75	*0.067*	11.6	4.2	2.2
rsd	*33*	*743*	27	5.7	*61*	12.4	42	*28*	15	42	*8.4*	50	81	57
min	*41*	*0.044*	408	184264	*13.6*	1.04	15.6	*5.3*	4.0	0.21	*0.063*	6.5	1.76	0.92
max	*89*	*1.33*	745	210997	*174*	1.24	40	*9.5*	5.8	0.92	*0.071*	19.7	9.7	3.7
Hz (2)	*10.8*	*0.90*	6151	6083	*5.3*	0.90	21	*2.3*	4.1	0.153	*0.62*	7.9	5.2	7.9
rsd	*103*	*132*	27	8.6	*64*	49	1.53	*16.7*	11.7	13.4	*1.47*	18.3	11.5	18
min	*2.9*	*0.061*	4998	5714	*2.9*	0.58	21	*2.0*	3.8	0.138	*0.62*	6.9	4.8	6.9
max	*19*	*1.73*	7304	6452	*7.7*	1.21	22	*2.6*	4.5	0.167	*0.63*	8.9	5.7	8.9
Polymict peridotite JJG1414														
Pn (9)	*23*	*0.135*	4159	4532	*6.5*	0.69	18.9	*10.9*	2.1	0.175	*0.22*	7.0	2.3	0.32
rsd	*222*	*96*	17.1	124	*205*	462	30	*100*	125	66	*152*	38	424	329
min	*6.7*	*0.044*	2781	167	*1.7*	0.31	10.8	*5.5*	1.027	0.104	*0.037*	6.4	0.94	0.182
max	*167*	*0.45*	5316	15429	*37*	8.2	29	*39*	7.6	0.33	*0.825*	13.0	31	3.4
Cp (2)	*105*	*1.01*	784	198308	*181*	<LOD	22	*21*	2.2	0.31	*((0.41))*	8.7	2.4	0.191
rsd	*57*	*113*	135	28	*129*		56	*53*	93	78		7.6	108	114
min	*63*	*0.20*	37	158920	*16*		13.3	*12.9*	0.76	0.140		8.2	0.56	0.037
max	*147*	*1.8*	1532	237696	*346*		31	*28*	3.71	0.48		9.2	4.2	0.35
Polymict peridotite JJG1513														
Po (2)	*168*	*0.064*	1363	1942	*6.0*	((0.39))	37	*5.3*	0.23	((0.116))	*((0.080))*	4.0	0.38	0.016
rsd	*64*	*109*	60	115	*57*		12	*52*	64			22	51	78
min	*92*	*0.0147*	783	368	*3.6*		34	*3.3*	0.129			3.4	0.24	0.007
max	*244*	*0.114*	1943	3515	*8.4*		40	*7.2*	0.34			4.6	0.52	0.025
Pn (1)	*228*	*0.34*	4242	10622	*72*	0.8	44	*4.2*	1.42			3.2	4.4	0.12

Mineral	*Re*	Os	Ir	Ru	Rh	Pt	Pd	Au
Ni-mineralised harzburgite XM1/422								
Native Ni (10)	*0.035*	3.0	1.28	2.1	0.21	0.24	0.125	0.020
rsd	*34*	165	322	497	1766	260	731	39

Table 2 (*continued*)

Mineral	*Re*	Os	Ir	Ru	Rh	Pt	Pd	Au
min	*0.028*	0.126	0.026	0.475	0.108	0.099	0.050	0.015
max	*0.051*	15.7	13.7	35	11.8	1.836	2.6	0.026
Hz (5)	*((0.017))*	2.7	1.46	0.28	0.23	0.141	0.100	((0.0076))
rsd		127	54	700	85	252	189	
min		0.118	0.130	0.136	0.044	0.107	0.074	
max		7.0	1.53	4.7	0.40	0.74	0.47	
Dj (4)	*((0.037))*	0.068	0.118	0.240	0.070	((0.069))	0.121	<LOD
rsd		42	29	48	70		77	
min		0.048	0.099	0.112	0.032		0.062	
max		0.089	0.174	0.38	0.130		0.25	
Phl-rich peridotite XM1/142								
Pn (14)	*0.092*	0.375	0.130	0.22	0.058	1.13	0.41	0.022
rsd	*30*	489	692	628	615	410	720	57
min	*0.046*	0.014	0.018	0.000	0.040	0.310	0.22	0.005
max	*0.154*	4.3	2.9	4.8	0.77	17.5	10.4	0.041
Phl-rich peridotite XM1/345								
Pn (3)	*0.38*	0.130	0.062	0.55	<LOD	0.071	0.41	0.159
rsd	*23*	46	49	19		46	46	97
min	*0.37*	0.045	0.026	0.43		0.067	0.39	0.153
max	*0.53*	0.159	0.085	0.64		0.125	0.72	0.42
MARID BLFX-3								
Pn (4)	*0.038*	0.162	0.115	1.167	0.027	0.060	0.054	0.021
rsd	*26*	98	35	12	43	118	159	2
min	*0.036*	0.050	0.058	1.121	0.013	0.018	0.046	0.020
max	*0.057*	0.27	0.142	1.43	0.037	0.157	0.197	0.021
Polymict peridotite DU-1								
Pn (6)	*0.023*	0.060	0.016	0.176	((0.0181))	0.198	0.055	0.032
rsd	*29*	20	121	23		81	57	44
min	*0.010*	0.051	0.009	0.131		0.014	0.033	0.019
max	*0.026*	0.069	0.052	0.242		0.41	0.077	0.049
Hz (2)	*0.009*	((0.0170))	0.021	0.088	<LOD	0.23	0.570	0.050
rsd	*94*		71	67		85	114	39
min	*0.0029*		0.0103	0.046		0.090	0.112	0.037
max	*0.014*		0.031	0.129		0.36	1.03	0.064
Cp (4)	*0.033*	<LOD	0.022	0.110	<LOD	0.052	((0.025))	na
rsd	*12.0*		22	40		63		
min	*0.032*		0.0186	0.079		0.029		
max	*0.039*		0.026	0.141		0.075		
	0.0							
Dg (1)	*0.0140*		0.0082	0.083		0.018	0.066	na
Polymict peridotite BD2666								
Pn (6)	*0.020*	0.057	0.034	0.31	0.026	0.092	0.134	0.020
rsd	*74*	159	71	42	13	65	200	52
min	*0.010*	0.049	0.0162	0.117	0.023	0.048	0.023	0.0121
max	*0.031*	0.21	0.082	0.43	0.030	0.20	0.75	0.039
Cp (4)	*0.028*	((0.028))	((0.028))	0.115	<LOD	0.044	0.127	0.029
rsd	*122*			35		17	38	913
min	*0.0043*			0.061		0.039	0.053	0.0188
max	*0.096*			0.139		0.050	0.159	0.550
Hz (2)	*0.027*	0.023	0.024	0.31	<LOD	0.074	0.23	0.085
rsd	*21*	12	53	7		7	14	49
min	*0.023*	0.021	0.0150	0.30		0.070	0.21	0.055
max	*0.031*	0.026	0.033	0.33		0.077	0.25	0.115
Polymict peridotite JJG1414								
Pn (9)	*0.047*	0.053	0.023	0.29	0.0188	0.30	0.117	0.024
rsd	*75*	31	46	17	20	242	307	271
min	*0.006*	0.027	0.012	0.21	0.0144	0.018	0.026	0.0048
max	*0.099*	0.069	0.044	0.33	0.022	1.73	1.07	0.182
Cp (2)		<LOD	0.015	<LOD	<LOD	0.31	((0.135))	((0.027))
rsd			13			112		
min			0.014			0.065		
max			0.017			0.558		
Polymict peridotite JJG1513								
Po (2)	*0.107*	0.23	0.25	0.32	0.056	<LOD	((0.0146))	0.026
rsd	*28*	17	5	49	64			49
min	*0.085*	0.20	0.24	0.212	0.031			0.017
max	*0.128*	0.26	0.26	0.43	0.082			0.035
Pn (1)	*0.053*	0.38	0.42	0.47		0.174	2.7	0.031

Median values from analyses of pure minerals (no inclusions or mixed sulphide analyses) with Si < 40000 ppm; Re corrected for co-ablation of serpentine (see Appendix 1).
Cp chalcopyrite, Dg digenite, Dj djerfisherite, Hz heazlewoodite, Pn pentlandite, Po pyrrhotite.
rsd relative standard deviation of n analyses given in parenthesis after mineral abbreviation, LOD limit of detection, double parentheses indicate that only a single value was >LOD, na not available (see Appendix 3); number in italics are semi-quantitative or include analyses that are semi-quantitative (see Appendix 1).

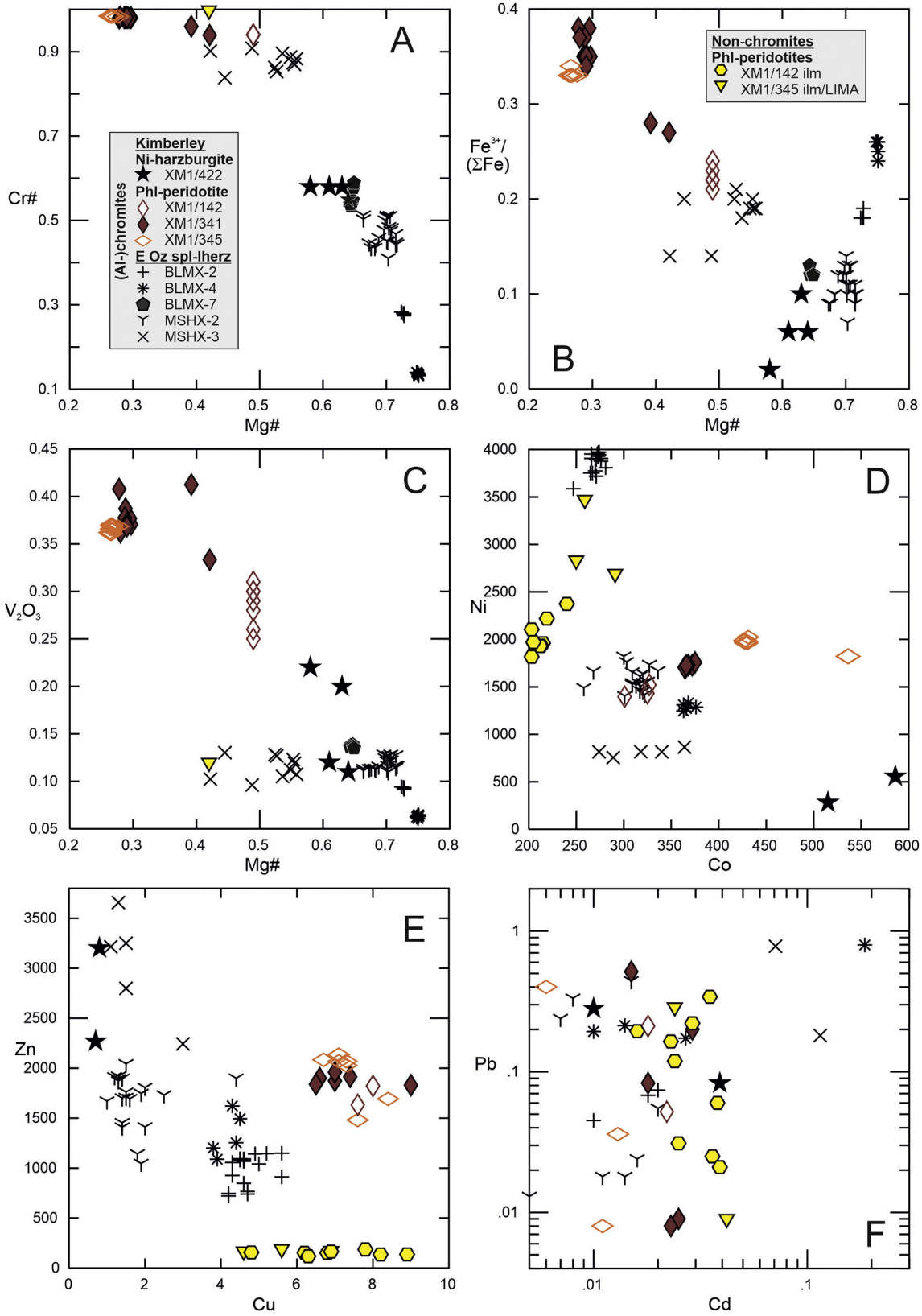

Fig. 6. Major-element (wt%) and trace-element (ppm) abundances as well as $Fe^{3+}/\Sigma Fe$ (calculated from stoichiometry), Mg# ($100Mg/(Mg+Fe^{total})$ and Cr# ($100Cr/(Cr+Al)$) in spinels and Ti-oxides (ilmenite ilm and LIMA) in Ni-enriched harzburgite (Ni-harz) and phlogopite-rich peridotite xenoliths (phl-perid) from Bultfontein as well as spinel-lherzolites from eastern Australia (Oz spl-lherz). All individual analyses are shown to illustrate major- and trace-element variability.

Table 3
Major- (wt%) and trace-element (ppm) concentrations in spinels and Ti-oxides in peridotite xenoliths from Bultfontein and eastern Australia.

Sample	Mineral	Comment	TiO_2	Al_2O_3	Cr_2O_3	V_2O_3	MgO	FeO	MnO	NiO	ZnO	Total	$Fe^{3+}/\Sigma Fe$	Mg#	Cr#
Spinel lherzolites, Oz															
BLMX2 Al chromite	Al-chromite		0.42	41.78	23.95	0.09	18.16	12.15	0.11	0.27	0.07	96.99	0.18	0.727	0.28
BLMX4 spinel avg (18)	spinel		0.31	52.13	12.12	0.06	19.82	11.75	0.09	0.37	0.08	96.74	0.26	0.750	0.13
BLMX7 Al chromite avg (5)	Al-chromite	variable Al, Cr	0.02	23.89	44.75	0.14	14.64	14.29	0.16	0.12	0.11	98.11	0.12	0.646	0.56
MSHX2-1 Al-chromite avg (15)	Al-chromite	variable Al, Cr, Fe	0.04	29.54	38.74	0.12	15.97	12.41	0.18	0.15	0.12	97.26	0.11	0.696	0.47
MSHX2-2 Al-chromite avg (6)															
MSHX3 chromite avg (5)	chromite		0.31	5.72	61.89	0.11	11.56	17.80	0.36	0.07	0.15	97.98	0.19	0.536	0.88
min			0.02	5.72	12.12	0.06	11.56	11.75	0.09	0.07	0.07		0.11	0.54	0.13
max			0.42	52.13	61.89	0.14	19.82	17.80	0.36	0.37	0.15		0.26	0.75	0.88
Ni-mineralised harzburgite															
XM1-422 chromite avg (2)	chromite~sympl		0.01	24.20	45.76	0.16	13.75	14.76	0.16	0.07	1.22	100.10	0.07	0.624	0.56
Phlogopite-rich peridotites															
XM1-341 chromite avg (6)	chromite		2.64	0.68	50.80	0.38	7.73	34.03	0.30	0.16	0.44	97.16	0.36	0.288	0.98
XM1-345 chromite avg (7)	chromite		2.66	0.59	51.95	0.37	7.12	34.84	0.30	0.18	0.15	98.16	0.33	0.267	0.98
XM1-142 chromite avg (3)	chromite		1.74	2.55	61.20	0.29	10.01	23.92	0.19	0.16	nd	100.04	0.22	0.427	0.94
min			1.74	0.59	50.80	0.29	7.12	23.92	0.19	0.16	0.15		0.22	0.27	0.94
max			2.66	2.55	61.20	0.38	10.01	34.84	0.30	0.18	0.44		0.36	0.43	0.98
Ti-oxides															
XM1-345 Ilm/LIMA avg (3)	ilmenite/LIMA		50.20	0.01	5.76	0.12	12.17	29.89	0.31	0.27	0.05	98.78	0.00	0.420	1.00
XM1-142 ilmenite avg (9)			na	na	na	na	na	na	na	na	na		na	na	na

Sample	*S*	Co	Ni	*Cu*	Zn	*Se*	Ru	Rh	Pd	*Ag*	*Cd*	*Te*	Os	Ir	Pt	*Au*	*Pb*	*Bi*
BLMX4	*6102*	270	3872	*4.7*	982	*0.83*	all <LOD	all <LOD	all <LOD		*0.013*	*0.048*	all <LOD	0.0004	0.0012	*na*	*0.069*	*0.002*
BLMX7	*1450*	367	1288	*4.2*	1331	*all <LOD*	all <LOD	all <LOD	all <LOD		*0.059*	*0.052*	all <LOD	0.0011	0.0013	*na*	*0.326*	*0.006*
MSHX2-1	*2546*	313	1586	*1.7*	1722	*0.60*	all <LOD	all <LOD	all <LOD		*0.013*	*0.050*	all <LOD	0.0003	all <LOD	*na*	*0.151*	*0.002*
MSHX2-2	*2469*	303	1542	*1.7*	1492	*all <LOD*	all <LOD	all <LOD	all <LOD		*0.015*	*0.026*	all <LOD	all <LOD	all <LOD	*na*	*0.187*	*0.002*
MSHX3	*1479*	317	814	*1.7*	3032	*all <LOD*	all <LOD	all <LOD	all <LOD		*0.081*	*<LOD*	all <LOD	all <LOD	all <LOD	*na*	*0.480*	*0.001*
min	*1450*	270	814	*1.7*	982	*0.60*					*0.013*	*0.026*		0.0003	0.0012		*0.069*	*0.001*
max	*6102*	367	3872	*4.7*	3032	*0.83*					*0.081*	*0.052*		0.0011	0.0013		*0.480*	*0.006*
XM1–422	*1434*	551	419	*0.77*	2735	*na*	all <LOD	all <LOD	all <LOD	*0.002*	*0.025*	*na*	all <LOD	0.002	0.042	*0.008*	*0.183*	*na*
XM1–341	*2032*	368	1724	*7.2*	1885	*na*	all <LOD	all <LOD	all <LOD	*na*	*0.022*	*0.036*	all <LOD	0.005	0.001	*na*	*0.142*	*0.002*
XM1–345	*1325*	429	1981	*7.4*	1936	*na*	all <LOD	all <LOD	all <LOD	*na*	*0.014*	*all <LOD*	all <LOD	0.0002	all <LOD	*na*	*0.414*	*0.002*
XM1–142	*680*	318	1449	*11.4*	1785	*na*	0.0007	0.0007	0.004	*0.20*	*0.015*	*na*	0.0005	all <LOD	0.038	*0.005*	*0.161*	*na*
min	*680*	318	1449	*7.2*	1785						*0.014*	*0.036*		0.0002	0.0012		*0.142*	*0.002*
max	*2032*	429	1981	*11.4*	1936						*0.022*	*0.036*		0.005	0.038		*0.414*	*0.002*
XM1–345	*1600*	267	2997	*5.7*	175	*na*	all <LOD	all <LOD	all <LOD	*na*	*0.031*	*all <LOD*	all <LOD	0.004	0.002	*na*	*0.148*	*0.005*
XM1–142	*639*	213	2031	*8*	150	*na*	0.001	0.003	0.008	*0.028*	*0.029*	*na*	0.002	0.003	0.036	*0.018*	*0.131*	*na*

Numbers in parentheses refer to number of trace-element analyses, median values are given, values in italics are semiquantitative except S which is qualitative, LOD is limit of detection, Mg# is $Mg/(Mg+Fe^{total})$ molar, Cr# is Cr/(Cr+Al) molar, na is not analysed number in italics are semi-quantitative or include analyses that are semi-quantitative (see text).

average TiO_2 contents (<LOD), V_2O_3 of 0.16 wt% and NiO of 0.05 wt% (Fig. 6; Table 3), whereas Ni-enriched spinel contains up to 5.7 wt% NiO (Giuliani et al., 2013a). By comparison, spinel in the three phl-peridotites is chromite, with TiO_2 ranging from 1.74 to 2.7 wt%, V_2O_3 from 0.29 to 0.38 wt%, and ZnO from 0.15 to 0.44 wt% (Fig. 6; Table 3). In two of these samples (XM1-341 and XM1-345), spinel coexists with ilmenite and LIMA, and sample XM1-341 hosts two generations of spinel, one of which has smaller grain size. The smaller-sized spinel, which potentially is of late origin, has higher TiO_2, Al_2O_3, Cr_2O_3 and MgO, but lower FeO content at similar V_2O_3 and ZnO compared to the larger spinel generation (Appendix 4).

For comparison, spinels and chromites in the eastern Australian spinel lherzolites (Oz-lherzolites hereafter) have generally lower TiO_2 (0.02–0.42 wt%), V_2O_3 (0.11–0.14 wt%) and ZnO contents (0.25–0.26 wt%), and are similar to Al-chromite in the Ni-harzburgite (Fig. 6; Table 3). One sample from Mt. Shadwell (MSHX-3) shows considerable heterogeneity with respect to major- and minor-element composition, although they all classify as chromites (Appendix 4). $Fe^{3+}/\Sigma Fe$ calculated from stoichiometry is low in spinel from the Ni-harzburgite (0.07) compared to those in phl-peridotites (0.22–0.36), while spinels in Oz-lherzolites have intermediate values (0.11–0.19). These values are broadly inversely correlated with Mg# ($Mg/(Mg+Fe^{total})$), and the Ni-harzburgite spinel is again more similar to the Oz-lherzolites spinels than to phl-peridotite spinels from Bultfontein (Fig. 6A; Table 3). Similar relationships apply to V_2O_3 concentrations in spinel, which are lowest in Oz-lherzolites (0.11–0.14 wt%) and the Ni-harzburgite (0.16 wt%), and highest in the phl-peridotites (0.29–0.38 wt%; Fig. 6C).

5.4. Spinel and Ti-oxide trace elements

Some individual grains and/or spot analyses in spinels from Oz-lherzolites MSHX2-1 and BLMX-7 are Cu-rich and are interpreted to contain contributions from minute sulphide inclusions. These analyses also have elevated Zn, Cd, Te, Pb and Bi, and quantifiable though low Os, Ir and Pt abundances, with Se mostly below detection limit (note that the concentrations of some of these elements are semi-quantitative, being calibrated against a Zn-Cu sulphide standard). The amount of included sulphide contributing to the volume sampled by the laser is minute. Extrapolating from measured Cu contents to 33 wt % Cu (in an assumed chalcopyrite inclusion) results in 7 ppm Os and 130 ppm each of Ir and Pt in the sulphide. The PGE concentrations calculated for the included sulphide therefore vastly exceed those determined (Table 2), but are well within the range of those determined for sulphide in other peridotite xenoliths from eastern Australia (Alard et al., 2000). The sulphide proportion is small, amounting to just 0.15 to 0.60 wt% sulphide for 500 to 2000 ppm Cu. Excluding these sulphide-contaminated analyses, average Co, Ni, Cu and Zn abundances in spinel are similar in Oz-lherzolites and Bultfontein phl-peridotites (310 vs. 370 ppm, 1820 vs. 1720 ppm, 2.8 vs. 8.7 ppm, 1710 vs. 1870 ppm), whereas the low-Ni spinel variety in the Ni-harzburgite shows higher Co (550 ppm) and Zn (2700 ppm), but lower Ni (420 ppm) and Cu (0.8 ppm; semi-quantitative values; Fig. 6; Table 3).

The PGE abundances in spinels are below detection limit or at most <5 ppb, with the exception of chromite from one of the phl-peridotites (XM1-142), which contains 38 ppb Pt. Of the other semi-quantitatively

determined siderophile-chalcophile elements, Cd, Te, and Bi abundances are low and similar in Oz-lherzolites and Bultfontein phl-peridotites (<50 ppb; Te and Bi not determined in Ni-harzburgite), whereas Pb abundances are in the 100s of ppb, again not showing discernible differences between different localities, despite significant differences in some minor-element concentrations, such as V_2O_3 (cf. previous section). The phl-peridotites contain ilmenite and LIMA, which were analysed in sample XM1-142 and XM1-345. These Ti-rich phases show similar Co, Zn, Cd and Pb abundances. In these samples, chromite has consistently higher V, Co, Cu (<2x), Pb (1–3x), much higher Zn (11–12x), but lower Ni (~0.7x) and Cd (~0.5x) abundances (Fig. 6; Table 3; Appendix 5).

5.5. Siderophile- and chalcophile-element distribution

The distribution of trace elements between sulphide, native Ni, spinel and Ti-oxide phases is summarised in Table 4 and shown in Fig. 7. In Ni-harzburgite XM1/422, the HSE are more abundant in native Ni, though highly variable, while heazlewoodite has similar IPGE and slightly lower PPGE, Re and Au. The IPGE abundances in the djerfisherite are >10x lower, but the difference is smaller for PPGE, and Au abundances are similar to those in native Ni (Fig. 7A). The HSE abundances in chromite are up to several orders of magnitude lower, with the exception of Pd and Au, which are within 10x of native Ni and the sulphide phases. With respect to the chalcophile elements, djerfisherite contains more Te, Ag, Mo and Pb, whereas heazlewoodite contains more Bi and As, and the spinels host more Zn than the other phases (Fig. 7A).

In the phl-peridotites, the abundances of most trace elements are orders of magnitude higher in pentlandite than in co-existing oxides (chromite and ilmenite/LIMA), with the exception of Au in XM1/142 and Zn in all phl-peridotites, which is again more abundant in the oxides than in pentlandite (Fig. 7B,C). Pentlandite, heazlewoodite and chalcopyrite in the polymict breccias show broadly similar HSE contents (Fig. 7D–E, G), but heazlewoodite is ≥10x enriched in Pd, Bi and Pb relative to the other sulphides. Pyrrhotite in one of the polymict breccias (JJG513) has generally lower trace-element abundances that are within 10x of those in the co-existing pentlandite, except >10 times lower Zn and Pb and >100x lower Pd (Fig. 7F).

5.6. Sulphide and native Ni modes

Sulphide modal abundances are estimated assuming that they host all S in the bulk rock. Bulk-rock compositions, which are available for the peridotites only (i.e. no polymict breccias), show S contents varying from 50 ppm in the Ni-harzburgite to 200 ppm in phl-peridotite XM1/341 (Holwell et al., 2019). These S contents fall within the range previously measured in kimberlite-hosted peridotite xenoliths (Fig. 8A), and are lower than the primitive mantle (PM) estimate of 200–250 ppm (McDonough and Sun, 1995; Palme and O'Neill, 2005). Assuming that all S resides in pentlandite (with 33 wt% S, in the phl-peridotites) and in heazlewoodite (with 25 wt% S, in the Ni-harzburgite), sulphides make up 0.02 to 0.06 wt% of the bulk rocks. These values are maxima if some S was added during post-emplacement alteration (Lorand and Grégoire, 2006), although the low bulk-rock S abundances argue against this.

The abundances of the strongly chalcophile element Te (whole-rock abundances reported in Holwell et al., 2019) can be used in a similar manner, and it is consistently <LOD in native Ni. The possible presence of tellurides, which are widespread in mantle peridotites (Delpech et al., 2012; König et al., 2015; Lorand et al., 2008, 2010; Lorand and Alard, 2010; Luguet et al., 2004), as discussed below, implies that estimates of sulphide modes from Te are maxima. Since high Te is associated with high S and Cu in bulk peridotites (Fig. 8B,C), Te abundances may be dominantly controlled by sulphide. The two approaches (i.e. using S and Te in bulk samples and median values in sulphides) result in variable sulphide modes, in part associated with high standard deviations, of 0.17 ± 0.16 wt% for pentlandite in phl-peridotite XM1/142, 0.043 ± 0.002 wt% for pentlandite in phl-peridotite XM1/345 and 0.023 ± 0.004 wt% for heazlewoodite plus djerfisherite in Ni-harzburgite XM1/422. A small proportion (10%, that is, 0.0023 wt%) of the estimated sulphide abundance in this sample is attributed to djerfisherite (Giuliani et al., 2013a), resulting in 0.021 wt% for heazlewoodite.

The abundance of native Ni can be estimated using Os concentrations, assuming that Os in harzburgite XM1/422 is solely hosted in native Ni and heazlewoodite. Bulk-rock Os abundances are not available, but Table 2 shows that the native Ni contains 3.0 ppm (albeit with large variability reflected in 1σ of ± 4.9 ppm). Almost as much Os resides in heazlewoodite (2.7 ± 3.5 ppm) and concentrations in djerfisherite and spinel are orders of magnitude lower or <LOD (Tables 2, 3). Even though IPGE are compatible in olivine (Mungall and Brenan, 2014) and spinel (Baumgartner et al., 2017; Locmelis et al., 2011; Pagé et al., 2012; Park et al., 2017), the distribution coefficients are orders of magnitude higher for sulphides and metals (Fleet et al., 1999; Peach et al., 1990), and partitioning into olivine or spinel is therefore ignored for the Ni-harzburgite. Having constrained the heazlewoodite mode to 0.021 wt% (previous paragraph), the abundance of native Ni is given by 0.021 wt% (heazelwoodite mode) × 3.0 ppm (Os in native Ni) / 2.7 ppm (Os in heazelwoodite) = 0.023 wt%, with a very large propagated uncertainty of ±0.050 wt% due to the variable Os abundances obtained for individual spot analyses in both native Ni and heazlewoodite.

Table 4
Trace-element distribution between native Ni, sulphides, spinels and Ti-oxides in peridotite xenoliths from Bultfontein.

Mineral pair	Sample	Co	Ni	Cu	Zn	As	Se	Mo	Ag	Cd	Sb	Te	Pb	Bi	Re	Os	Ir	Ru	Rh	Pt	Pd	Au
pn/cp	DU-1	38	17.0	0.051	0.18	0.72	1.10	0.77	0.92	0.76	2.95	0.92	3.0	1.67	0.71	na	0.72	1.60	na	3.8	2.2	na
pn/cp	BD2666	7.4	4.0	0.024	0.054	0.69	0.41	0.54	0.27	0.14	0.46	0.56	0.62	2.9	1.4	2.0	1.19	2.7	na	2.1	1.06	0.70
pn/cp	JJG1414	5.3	4.5	0.023	0.036	na	0.86	0.53	0.92	0.56	0.54	0.80	0.97	1.69	na	na	1.51	na	na	0.95	0.87	0.90
pn/po	JJG513	3.1	3.4	5.5	11.9	2.1	1.18	0.80	6.06	na	na	0.81	11.5	7.5	0.5	1.69	1.68	1.47	na	na	185	1.21
pn/hz	DU-1	2.4	0.52	2.8	0.12	0.56	1.00	0.68	0.82	1.27	0.089	0.93	0.09	0.22	2.70	3.5	0.78	2.0	na	0.88	0.10	0.64
pn/hz	BD2666	0.65	0.55	0.76	1.09	0.88	0.56	1.64	0.34	0.68	0.050	0.82	0.49	0.81	1.03	2.4	1.41	0.99	na	1.24	0.59	0.23
Native Ni/hz	XM1/422	1.6	1.3	4.7	1.0	0.035	na	0.78	0.87	0.67	0.078	na	0.0	0.0	2.1	1.08	0.88	7.5	0.90	1.72	1.24	2.7
Native Ni/dj		0.51	3.6	0.59	0.61	2.3	na	0.075	0.016	1.98	1.00	na	0.020	0.003	0.95	43	10.8	8.8	2.9	3.5	1.03	na
cp/dg	DU-1	1.13	2.2	0.79	6.3	2.6	4.6	0.98	0.83	2.9	0.97	1.72	1.77	1.31	2.36	na	2.7	1.33	na	2.9	0.39	na
hz/chr	XM1/422	3.6	1689	919	0.007	na	na	na	101	36	na	na	447	na	na	na	na	na	na	3.4	na	0.99
pn/chr	XM1/345	18.5	210	2553	0.015	na	na	na	na	24	na	na	65	602	na	na	na	na	na	na	na	na
pn/chr	XM1/142	8.0	193	412	0.058	na	na	na	43	58	na	na	279	241	na	750	na	312	83	30	104	4.1
pn/ilm-LIMA	XM1/345	30	138	3314	0.169	na	na	na	na	10.6	na	na	183	na	na	na	16.0	na	na	36	na	na
pn/ilm-LIMA	XM1/142	12.0	138	588	0.69	na	na	na	313	30	na	na	343	na	na	187	43	219	19.5	32	52	1.25

Values from Tables 2 and 3 (=medians) were used for calculation, note that Zn, Mo, Sb and Re are semi-quantitative in sulphide, as applies to Cu, Ag, Cd, Au, Pb and Bi in oxides; na not available (not measured or values <limit of detection).
Cp chalcopyrite, dg digenite, dj djerfisherite, hz heazlewoodite, pn pentlandite, po pyrrhotite, chr chromite, ilm ilmenite.

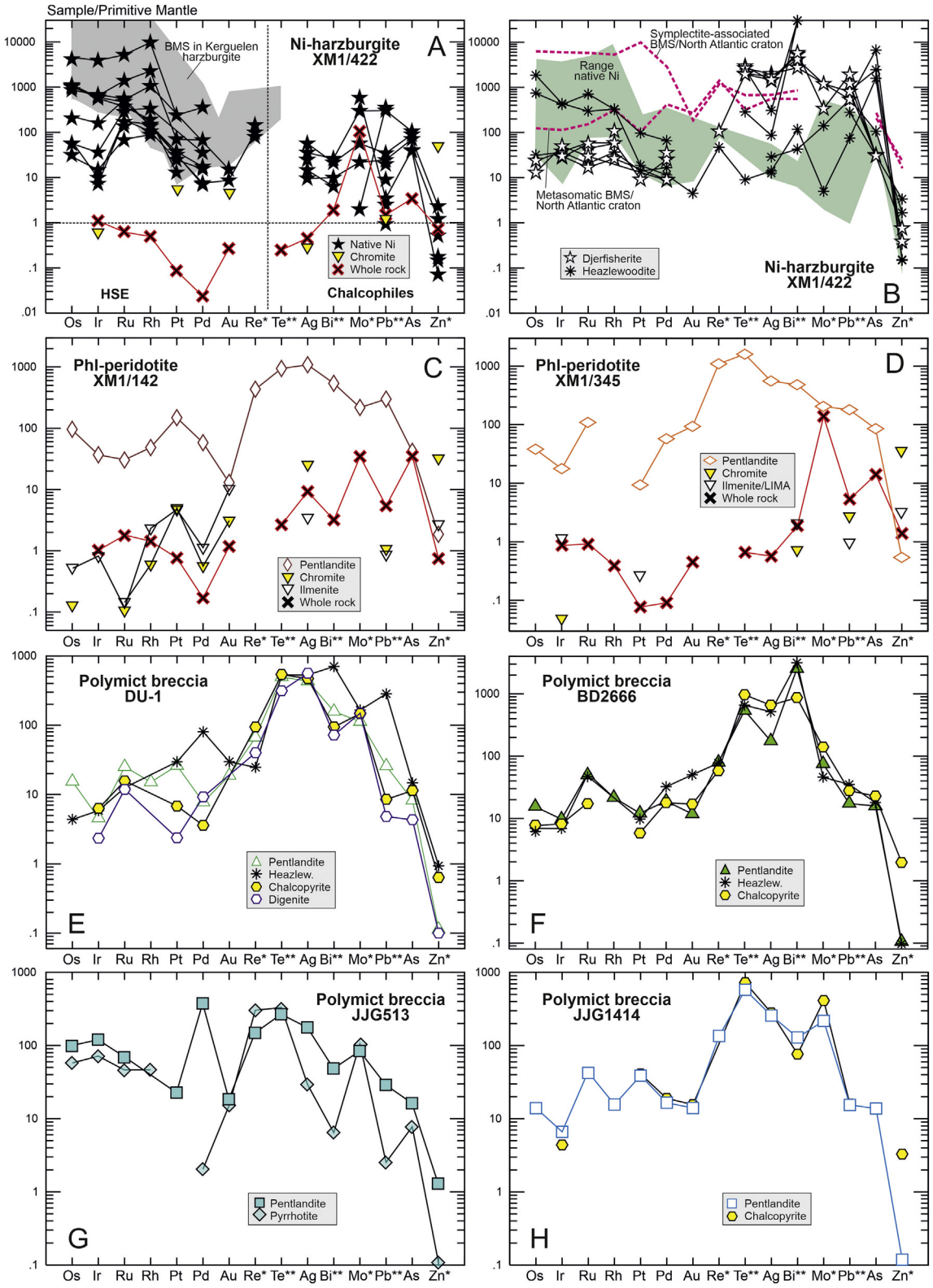

Fig. 7. Primitive mantle-normalised HSE and trace element patterns showing concentrations in native Ni, sulphides, and spinels plus Ti-oxides in Ni-enriched harzburgite, phlogopite-rich peridotites and polymict breccia xenoliths from Bultfontein. * denotes semi-quantitative determination for sulphides, ** denotes semi-quantitative determination for spinels and oxides (see Appendix 1 for details). All individual analyses are shown for native Ni and sulphides in the unusual Ni-enriched harzburgite to illustrate the range of compositions. Medians and average values are shown for other sulphides and oxides, respectively. Shown for comparison in A. and B. are compositions of sulphides in a harzburgite xenolith from Kerguelen (Delpech et al., 2012) and average compositions of PGE-rich sulphide associated with symplectite and PGE-poor interstitial sulphide in a spinel lherzolite peridotite from the North Atlantic craton in Scotland (Hughes et al., 2017), respectively. Whole-rock compositions available for some of the samples are from Holwell et al. (2019). Element order of the HSE is from most to least compatible by convention, whereas the order of the other siderophile and chalcophile elements reflects decreasing median primitive mantle-normalised concentrations in pentlandite derived in this study. Primitive mantle values from McDonough and Sun (1995), Becker et al. (2006) and Fischer-Gödde et al. (2011).

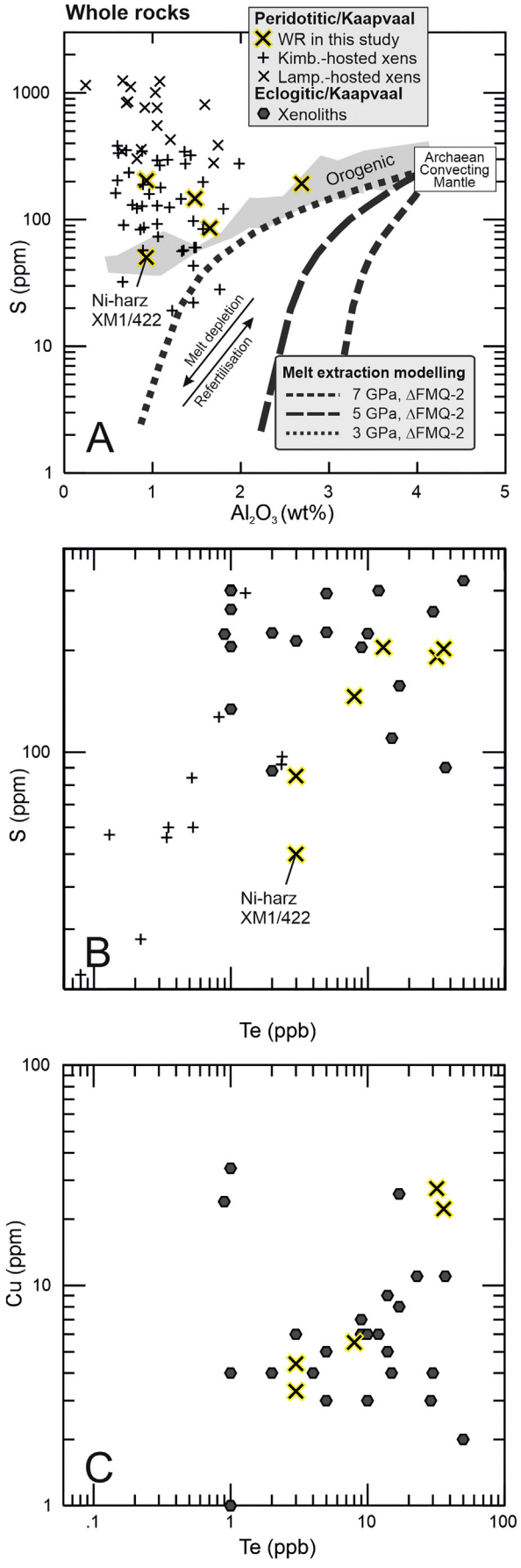

Fig. 8. A. Whole-rock Al_2O_3 (wt%), a proxy of melt depletion, vs. S concentration (ppm) in kimberlite- and lamproite- (formerly orangeite) borne peridotite xenoliths from southern Africa (Maier et al., 2012; Pearson et al., 2004), and in metasomatised peridotites from Bultfontein targeted in this study (data from Holwell et al., 2019). Shown for comparison are melting contours for melt extraction from Archaean convecting mantle from Aulbach et al. (2016), illustrating that all depicted xenoliths are expected to have lost their sulphide complement during initial melt depletion, and that they were subsequently resulphidised. Arrows qualitatively show the trends for melt depletion and refertilisation via addition of Al_2O_3-bearing minerals, such as spinel and clinopyroxene. B. Sulfur concentrations (ppm) as a function of Te (ppb) in whole rocks as in A., plus Kaapvaal eclogite xenoliths from Gréau et al. (2013). Samples in the present study are enriched in S and Te compared to other southern African peridotite xenoliths and more similar to eclogite xenoliths. C. Cu concentrations (ppm) in whole rocks as a function of Te (ppb).

6. Discussion

6.1. Spinel in continental lithospheric mantle: a sulphide attractor?

Whether PGE are spinel-compatible or not in the mantle remains debated. Quantifiable PGE abundances (in particular IPGE) in spinel may relate to incorporation into the structure (e.g., Arguin et al., 2016; Baumgartner et al., 2017; Brenan et al., 2012; Locmelis et al., 2011; Pagé et al., 2012; Park et al., 2012, 2017; Righter et al., 2004). This is supported by the absence of PGE atomic clusters even when actively searched for by Transmission, Analytical and Scanning-Transmission Electron Microscopy in harzurgitic Cr-spinel containing measurable PGE abundances (5.70 ppb Os, 6.36 ppb Ir, 10 ppb Ru, 9.11 ppb Pt, 1.02 ppb Pd; Ferraris and Lorand, 2008). The latter study further indicates that the IPGE and Pt, but not Pd, preferentially partition into Cr spinel relative to silicate melt. Alternatively, elevated PGE abundances reflect co-ablation of micrometric sulphide or PGM inclusions, which in chromite are commonly from the laurite-ehrlichmanite series (RuS_2-OsS_2) or IPGE alloys (e.g., Fiorentini et al., 2004; González-Jiménez et al., 2009; Kamenetsky et al., 2015; Kutyrev et al., 2020). Certain PGE deposits are associated with chromite, which may trap PGM at the mineral melt interface due to strong oxygen fugacity gradients caused by the formation of Fe^{3+}-bearing spinel (Finnigan et al., 2008).

In the xenoliths under study, spinel and Ti-oxide phases appear to lack micrometric PGM inclusions, as trace-element abundances in analyses free of sulphide are relatively constant and PGE abundances are commonly <LOD (Table 3, Appendix 5). This does not preclude the presence of nanometric inclusions, which will not show up in time-resolved LAM-ICPMS analyses. Abundances are similarly low in chromite in peridotite xenoliths from the North China Craton (Wu et al., 2006), and show little overlap with HSE contents in ophiolite-associated chromite ores (Gervilla et al., 2005), which approach HSE concentrations similar to pentlandite in this study (Fig. 9A). Thus, spinel in cratonic mantle assemblages is generally an insignificant structural host of the HSE. Exceptions are the abundances of Pt and Au in chromite from the Ni-harzburgite, which are within an order of magnitude of sulphide and native Ni in the same sample (Fig. 7A), and Au abundances in ilmenite and chromite, which are nearly as high as in pentlandite in Phl-peridotite XM1/142 (Fig. 7B). This is consistent with observations from other dynamic settings, as Al-spinel from fertile orogenic mantle lherzolite is PGE-poor (Os 0.009–0.227, Ir 0.095–0.261 ppb, Pt 0.29–0.63, Pd 0.22–0.46 ppb) with a single reliable Ru analysis yielding 1.33 ppb (Lorand et al., 2008).

Low PGE abundances may in part relate to the low-fO_2 conditions (generally below the fayalite-magnetite-quartz buffer FMQ; e.g., Woodland and Koch, 2003; Yaxley et al., 2017) that generally predominate in the cratonic lithospheric mantle, even in metasomatised assemblages. Low fO_2 may inhibit PGE partitioning into spinel (Brenan et al., 2012; Park et al., 2017), though some continental mantle samples are more oxidised (e.g., Rielli et al., 2017, 2018a, 2018b). Also, even peridotites yielding relatively high fO_2 of FMQ-1 contain PGE-poor Cr-spinels (≤10 ppm), despite their highly refractory composition, with

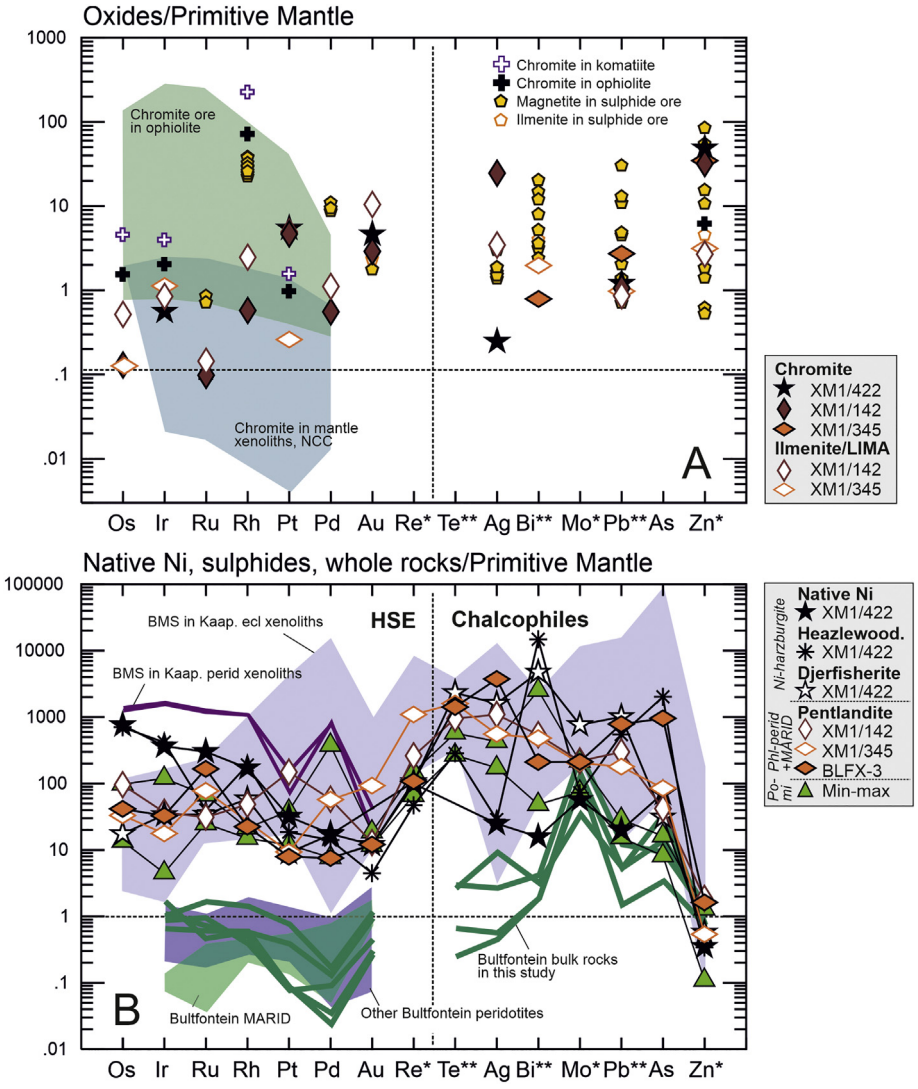

Fig. 9. Primitive-mantle normalised HSE and trace element patterns showing minerals in Ni-enriched harzburgite, phlogopite-rich peridotites (Phl-perid), MARID and polymict breccia (Po-mi) xenoliths from Bultfontein. A. Spinels and Ti-oxides. Shown for comparison are range of HSE concentrations in chromite in peridotite xenoliths from the North China craton (Wu et al., 2006) and in chromite ore associated with ophiolite (Gervilla et al., 2005), as well as chromite in komatiite and in ophiolite (Arguin et al., 2016; Pagé and Barnes, 2016), and magnetite and ilmenite in sulphide ores (Dare et al., 2012). B. Median concentrations in native Ni, heazlewoodite, djerfisherite and pentlandite (range is shown for polymict breccias for clarity). Shown for comparison are the range of mss compositions in eclogite xenoliths (Burness et al., 2020) and mss in peridotite xenoliths (Alard et al., 2000) from the Kaapvaal craton, bulk compositions for Bultfontein xenoliths investigated in this study (Holwell et al., 2019) and range of bulk compositions for MARID and for other Bultfontein xenoliths investigated in an earlier study (Maier et al., 2012). Primitive mantle values from McDonough and Sun (1995), Becker et al. (2006) and Fischer-Gödde et al. (2011).

≤1.22 wt% Al_2O_3 (Luguet et al., 2007). Of the trace elements analysed in both sulphide and spinel phases, only Zn, Cd and Pb are consistently >LOD, and these elements are 10x to 100x more abundant in pentlandite or heazlewoodite than in chromite or ilmenite/LIMA. Thus, oxides are, unsurprisingly, insignificant hosts also of the chalcophile elements in cratonic peridotite xenoliths.

In contrast, spinel with suspected sulphide inclusions (Ozlherzolites MSHX2-1 and BLMX-7), based on elevated Cu contents, also displays quantifiably higher Os, Ir and Pt abundances (Fig. 10A,B), testifying to the chalcophile nature of these elements and their preferred partitioning into sulphide relative to oxide phases. Conversely, Ru, Rh and Pd remain entirely below the LOD, also in the analyses of sulphide-contaminated spinel. In the lithospheric mantle, spinel, sulphide and clinopyroxene are commonly interpreted to precipitate together during silicate melt metasomatism (e.g., Lorand et al., 2013; Wittig et al., 2010). This may have also occurred in the metasomatised peridotites from Bultfontein investigated in this study, as spinel, sulphide and clinopyroxene are texturally associated with phlogopite (Table 1). Micro-scale composition-fO_2 gradients at ≥FMQ+0.5 in the melt (Jugo et al., 2010) and/or FeO gradients ensuing from spinel precipitation may have favoured localised sulphide saturation, as the S content in melt at sulphide saturation is strongly FeO-dependent (Wykes et al., 2015).

6.2. Main siderophile- and chalcophile-element hosts in metasomatised peridotites

Bulk-rock HSE and trace-element compositions are available for three samples in this study (Ni-harzburgite XM1/422 and phl-peridotites XM1/142 and XM1/345; data in Holwell et al., 2019). Combined with sulphide mode estimates (Section 5.6) and determination of trace elements in native Ni and in Ti-oxide, spinel and sulphide phases, bulk-rock data permit to determine how siderophile and chalcophile elements are distributed between the minerals (Table 4), including whether or not additional hosts are required (Table 5). Primitive Upper Mantle-normalised (hereafter denoted with subscript PUM) trace-element abundances for minerals and whole rocks in individual samples are displayed in Figs. 7 and 9.

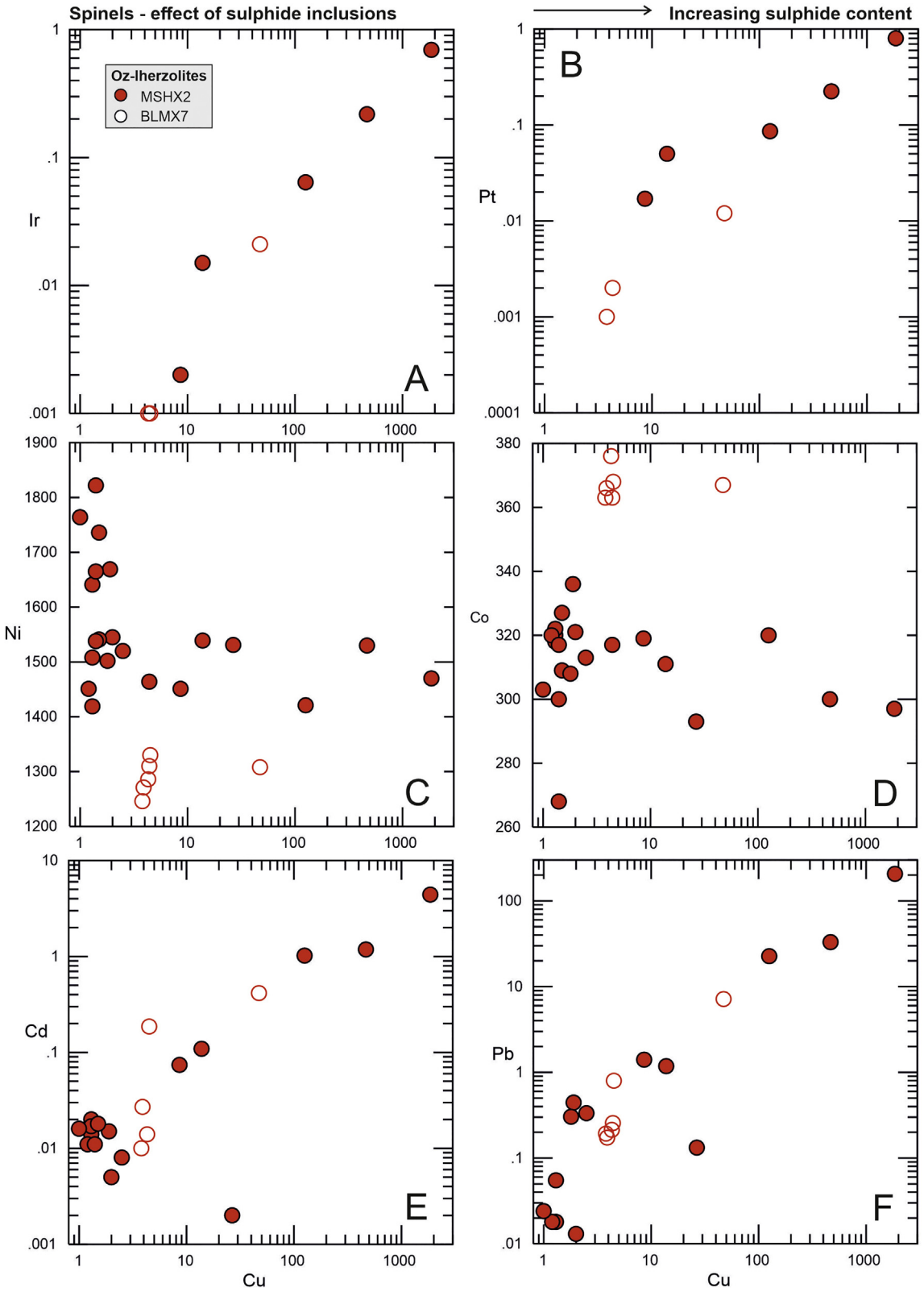

Fig. 10. Trace-element abundances (ppm) of spinels in lherzolite xenoliths from eastern Australia as a function of Cu, illustrating the effect of suspected chalcopyrite inclusions (gauged by elevated Cu content) on the abundances of chalcophile elements.

6.2.1. Highly siderophile elements

Table 5 illustrates that, except for Pd (20–50%) and Pt in one phl-peridotite (30%), only a small proportion of the PGE (<25%; Os abundances in whole rocks are not reported) is accommodated in sulphide and native Ni in the Ni-harzburgite or in pentlandite in the phl-peridotites, and <10% of Au can be accounted for. As discussed in the previous section, spinels and Ti-oxides in xenoliths are insignificant hosts of HSE. Thus, additional carriers are required even if maximum

Table 5
Proportions of siderophile and chalcophile elements in the whole rock hosted by sulphides and native Ni.

Sample	Mode wt%	Co	Ni	Cu[b]	Zn[a]	As	Mo[a]	Ag	Cd[b]	Sb[a]	Te[b]	Pb[b]	Bi[b]	Ir	Ru	Rh	Pt	Pd	Au
XM1/422 WR (ppm)		80	1721	3.3	40	0.17	5.3	0.004	0.01	0.034	0.003	0.23	0.005	0.0039	0.0047	0.0006	0.0007	0.0002	0.0005
% in hz	0.021	0.51	8.57	4.47	0.010	12.28	0.01	1.32	3.1	4.52	24	7.54	161	7.86	1.24	7.9	4.5	12.3	0.35
1σ	0.004	0.11	1.84	0.96	0.002	2.64	0.00	0.28	0.7	0.97	5	1.62	35	1.69	0.27	1.7	1.0	2.6	0.07
% in dj	0.0023	0.18	0.34	3.97	0.002	0.02	0.02	8.14	0.1	0.04	22	1.55	6	0.07	0.12	0.3	0.2	1.6	na
1σ	0.0005	0.04	0.07	0.85	0.000	0.00	0.00	1.75	0.0	0.01	5	0.33	1	0.02	0.03	0.1	0.1	0.4	
% in native Ni	0.02	0.90	11.93	23.49	0.011	0.48	0.01	1.27	2.3	0.39	na	0.31	0	7.69	10.37	8.0	8.5	17.0	1.03
1σ	0.05	1.96	25.90	51.00	0.024	1.05	0.03	2.76	5.0	0.85		0.66	0	16.70	22.51	17.3	18.5	36.9	2.24
Sum in native Ni+sulphides		1.59	21	32	0.023	12.8	0.04	10.7	5.6	5.0	45	9.4	167	15.6	11.7	16.2	13.2	31	1.37
XM1/142-B WR (ppm)		62	1123	28	41	1.75	1.73	0.07	0.02	0.05	0.032	0.82	0.01	0.0036	0.0118	0.0017	0.0058	0.0012	0.0020
% in pn	0.17	6.97	42.18	28.96	0.423	0.20	1.07	19.91	7.2	0.31	60	9.33	29	6.13	3.14	5.7	33.1	58.0	1.85
1σ	0.16	6.49	39.27	26.96	0.394	0.19	1.00	18.54	6.7	0.28	56	8.68	27	5.71	2.92	5.4	30.8	54.0	1.73
XM1/345 WR (ppm)		114	1885	5.5	77	0.71	7.0	0.00	0.01	0.03	0.008	0.81	0.00	0.0031	0.0066	0.0005	0.0006	0.0007	0.0008
% in pn	0.043	3.00	9.46	147.61	0.017	0.26	0.06	41.75	1.0	0.63	103	1.43	11	0.87	3.57	na	5.2	26.9	8.85
1σ	0.002	0.12	0.39	6.15	0.001	0.01	0.00	1.74	0.0	0.03	4	0.06	0	0.04	0.15		0.2	1.1	0.37

WR whole rock, hz heazlewoodite, dj djerfisherite, pn pentlandite; whole-rock abundances from Holwell et al. (2019).
Sulphide and native Ni modes as well as uncertainties were derived as described in the text.
[a] Semi-quantitative determination for sulphides.
[b] Semi-quantitative determination for oxides (see Appendix 1 for details).

proportions of sulphides and native Ni within the uncertainty are assumed. Studies of postcratonic mantle peridotites have repeatedly shown that Au does not necessarily reside in BMS (e.g. Delpech et al., 2012; Lorand et al., 1999, 2008, 2010). Indeed, micrometric inclusions of novodneprite ($AuPb_3$) and anyuiite, $Au(Pb,Sb)_2$, together with nanometric clusters of metallic Au were detected in olivine in lherzolites from Lherz using Transmission Electron Microscopy (TEM) and Electron Energy Loss Spectroscopy (EELS) (Ferraris and Lorand, 2015).

Being typically minute and easy to overlook (e.g., Kamenetsky et al., 2015; Kamenetsky and Zelenski, 2020; Lorand et al., 2010; Luguet et al., 2007), PGM inclusions in sulphides are nonetheless commonly recognised in time-resolved element spectra from LAM-ICPMS analyses (e.g., Griffin et al., 2002; Savelyev et al., 2018). In the present study, indirect observation of PGE- or semimetal-rich "nuggets" in the sulphides is also based on the presence of signal spikes or more sustained elevated signals in the time-resolved spectra of sulphide minerals (listed as "inclusions" in Appendix 3, example spectra in Appendix 6). Sub-micron Pt-Fe alloy grains with enrichment also in Re have previously been observed as inclusions in sulphide in a harzburgite xenolith from Bultfontein where they were ascribed to exsolution during subsolidus re-equilibration (Wainwright et al., 2016). Conversely, native Ni appears to be free from such inclusions, at least at the micron-scale resolution permitted by optical methods, SEM or the duration of one element sweep during LAM-ICPMS analysis. A Pt-Au inclusion is observed by electron microscopy in heazlewoodite, itself included in the margin of an olivine grain, in Ni-harzburgite XM1-422 (Fig. 2H–I).

These observations support the conclusion that significant portions of the PGE and Au are hosted in micro- and nano-phases, which may include combinations with Te, As, Sb and Bi (collectively referred to as TABS; Mansur et al., 2019) in addition to PGE alloys (Helmy and Botcharnikov, 2020). The involvement of TABS during both refertilisation and cryptic metasomatism, leading to formation of discrete Pt-Pd-Te-Bi microphases, has long been recognised in postcratonic mantle (Delpech et al., 2012; König et al., 2015; Lorand et al., 2008, 2010; Lorand and Alard, 2010; Luguet et al., 2004). This has been complemented by experimental studies investigating the phase relations of these minerals, and PGE behaviour under varying conditions (Helmy et al., 2007, 2010, 2013; Helmy and Botcharnikov, 2020; Helmy and Bragagni, 2017). There is some evidence that such phases occur as microinclusions in heazlewoodite from the Ni-harzburgite, and they may additionally occur interstitially where they cannot be sampled by LAM-ICPMS. Such grains either crystallise from an incompatible element-enriched residual sulphide liquid or exsolve from base-metal sulphides, especially after S-loss (Mansur et al., 2019; Mansur and Barnes, 2020). Exsolution can explain the observation of co-ablated Pd-Pt-Au-rich inclusions, whereas discrete micro-nuggets (we re-emphasise that parts of the spectra showing evidence for such micronuggets were excluded for trace-element quantification in the sulphides reported in Table 2) can help explain the deficits in measured grains (Table 5).

6.2.2. Moderately and slightly siderophile elements (V, Cr, Mn, Co, Ni, Cu, Zn, Mo)

Some 25 to 100% of Cu can be accounted for by sulphide, suggesting that Cu is only weakly lithophile (Table 5). In contrast, the abundances of other moderately and slightly siderophile elements (V, Cr, Mn, Co, Ni, Mo), with the notable exception of Zn, are not elevated or depleted in spot analyses of spinel with assumed co-ablation of sulphide. These elements thus do not strongly prefer a sulphide over an oxide mineral host, in accord with their partially lithophile nature, which allows them to bond with both sulphur and oxygen (Wood and Kiseeva, 2015). Moreover, Mo, Ni and Co in the bulk rocks are unaccounted for by either native Ni or sulphide phases, despite being enriched in these minerals compared to primitive mantle or bulk rocks (Fig. 7). Consequently, a proportion of these elements probably is hosted in the modally dominant silicates (e.g., 10s of ppm Co, 100s of ppm V in clinopyroxene, 100s of ppm Co and Zn, and 1000s of ppm Ni in olivine from cratonic peridotite xenoliths; Griffin et al., 1989; Aulbach et al., 2017), making sulphides, spinels or Ti-oxides insignificant hosts of these elements in view of their typically low modal abundances in mantle xenoliths.

6.2.3. Chalcophile elements and chalcogens (As, Se, Cd, Sb, Te, Pb, Bi)

The abundances of Cd, Te, Pb and Bi are elevated in the sulphide-contaminated spot analyses in spinel (some shown in Fig. 10E,F). These are among the group of elements identified as becoming more chalcophile under low oxygen fugacities (Ag, Cd, Hg, In, Pb, S, Se, Te, and Zn; Barnes, 2016). Table 5 shows that Te, along with As, Ag, Cd, Sb and in part Bi, require additional hosts. This reinforces the suggestion that tellurides, and possibly bismuthinides, antimonides and other micro- or nano-phases are required to account for part of the chalcophile element budget along with some HSE (see above).

Indeed, micro-inclusions of minerals with high concentrations of chalcophile elements have been identified in time-resolved spectra, such as Cd-rich inclusions in two different pentlandite grains in phl-peridotite XM1/341, and As-Te-Sb inclusions and an Ag inclusion in heazlewoodite grains in Ni-harzburgite XM1/422 (some example

spectra in Appendix 6). Inclusions of gersdorffite (NiAsS), native Cu and Cu sulphides occur in heazlewoodite in this sample (Giuliani et al., 2013a). Lorand and Grégoire (2006) describe micron-sized Ni sulfide particles dispersed throughout the serpentinised matrix of mantle xenoliths from Bultfontein and nearby localities. Therefore, there likely is an additional role for a grain-boundary sulphide component, too fine-grained to be sampled by LAM-ICPMS, in balancing some of the chalcophile element budget, as suggested for cratonic mantle xenoliths elsewhere (e.g., Aulbach et al., 2019; Hughes et al., 2017).

6.3. Effects of low-temperature processes on siderophile and chalcophile element mobility

6.3.1. Trace-element redistribution during subsolidus re-equilibration

Subsolidus exsolution of pyrrhotite, pentlandite and chalcopyrite from a high-temperature monosulphide has affected all sulphides in kimberlite-borne mantle xenoliths from the Kaapvaal Craton, as reviewed in Lorand and Grégoire (2006). This assemblage is recognised in the polymict breccias (Table 1), where pyrrhotite in only one sample could be analysed (JJG513). The pyrrhotite has generally low trace-element abundances, within 10x of those in the co-existing pentlandite, except for >10 times lower Zn, Pb and even lower Pd (0.015 ppm compared to 2.7 ppm in pentlandite; Tables 2, 4), consistent with the affinity of pentlandite for Pd (Lorand et al., 2013). Conversely, chalcopyrite is consistently enriched (1.3 to 1.9x) in Te, Ag, Mo, As and Au, and >10x in Zn and depleted in Bi (2x), whereas the PGE are either slightly depleted or similar to those in pentlandite it coexists with (Fig. 7). Considering these systematics, and assuming low-temperature equilibration is an isochemical process, the abundances of PGE will be higher in pentlandite than in the corresponding bulk sulphide.

6.3.2. Serpentinisation and desulphurisation

Serpentinisation leads to a decrease in S/metals at high Ni/Fe in sulphide, which contrasts with the effects of supergene alteration described from eclogite xenoliths from the Kaapvaal Craton, which caused an increase in both S/metals and Ni/Fe in sulphide (Gréau et al., 2013). In the present study, evidence for late-stage desulphurisation includes the presence of texturally unequilibrated secondary sulphide minerals, such as heazlewoodite after pentlandite (Fig. 4D) or digenite after chalcopyrite, and of finely intergrown magnetite and serpentine in the remnant "primary" sulphide mineral grains (e.g., Fig. 4A,D,G) as well as the presence of native Cu (Section 3 and Giuliani et al., 2013b). Veinlets, apophyses and trails of Ni-sulphides are interpreted as further manifestations of this process (Fig. 2A–C, G, Fig. 4D). In xenoliths from kimberlites on Somerset Island, submicron-sized PGM appear associated with serpentinisation (Bragagni et al., 2017). However, the single Pt "nugget" detected visually in sample XM1/422 occurs in heazlewoodite included in the margin of an olivine grain adjacent to a serpentine-filled fracture (Fig. 2I).

Recent work on partially serpentinised peridotites associated with ophiolite indicates that Ag, Au and PPGE migrate from pentlandite to newly formed Cu and Fe metal, with little mobilisation at the hand specimen scale (Lawley et al., 2020a). Except in the Ni harzburgite, such metals are not observed in samples in this study. Similarly, Westner et al. (2019) find that surficial weathering and associated sulphide breakdown in peridotite xenoliths has little effect on their PGE systematics. However, heazlewoodite replacing primary pentlandite in two polymict breccias (DU-1 and BD2666) has consistently higher As, Ag, Sb, Te, Bi, Pb and Au and lower Os. The distribution is variable for the remaining elements (Co, Cu, Zn, Se, Mo, Cd, Re, Ir, Ru and Pt; Table 4). The higher siderophile and chalcophile element contents in heazlewoodite could imply that serpentinisation is a non-isochemical process, reflecting efficient transport in the serpentinising fluid after scavenging of these elements elsewhere in the system during partial desulphurisation.

6.4. New insights into the origin of Ni-rich zones in mantle peridotite

6.4.1. Formation conditions

The processes leading to formation of Ni-rich assemblages at mantle depths remain unclear (Giuliani et al., 2013a; Lorand and Grégoire, 2006). The spatial association of native Ni with minor apatite, aegirine and djerfisherite, as well as carbonates and halides, together with the pyroxene-poor nature of the Ni-enriched zones and the presence of carbonate-rich fluid inclusions, suggests the involvement of an alkali- and volatile-rich, carbonated small-volume melt or fluid (Giuliani et al., 2013a). This melt is required to be HS^--poor because phase relationships at T > 625 °C would otherwise favour the formation of a Ni-sulphide melt (Lorand and Grégoire, 2006). Although the equilibration temperatures derived for the Ni-harzburgite (670 to 720 °C) are not much above this threshold, the low abundance of djerfisherite relative to metal in the metasomatised zone argues in favour of an S-limited environment, with low fS_2. Ni-rich zones with diffusive halos (Fig. 2A,C,E) indicate that not enough time was available for chemical re-equilibration, thus suggesting a temporal link with host kimberlite magmatism. Moreover, they suggest that Ni-enrichment occurred at sufficiently high temperatures for volume diffusion, consistent with a mantle origin rather than a near-surface origin related to serpentinisation (Giuliani et al., 2013a). Nickel-enriched minerals are spatially associated with symplectites of Cr-spinel ± clinopyroxene ± enstatite related to garnet breakdown, which may have provided mechanically weak zones for fluid ingress (Giuliani et al., 2013a). In the Scottish part of the North Atlantic Craton, a PGE-rich sulphide with much higher Pt and Pd contents than native Ni or sulphide phases in the Ni-harzburgite (Fig. 7A,B) is also associated with symplectites, and has been linked to an event involving immiscible carbonate-sulphide-phosphate fluids or melts (Hughes et al., 2017).

Brines have been shown to efficiently mobilise Pt and Au (Hanley et al., 2005). Since Cl was certainly abundant in the melt, judging by the presence of chlorides and Cl-bearing apatite, phlogopite and djerfisherite (Giuliani et al., 2013a), the question arises whether the siderophile elements were mobilised by the metasomatic agent. However, the concentrations of Pt and Au are low or undetectable in native Ni and djerfisherite (Table 2). Moreover, at least at low pressures, the transport of Pt (and Pd) as chloride complexes requires extremely acidic and oxidising conditions (Barnes and Liu, 2012), which appear to be precluded by the presence of calcite and alkali carbonates in the Ni-rich assemblage. Conversely, Cl enrichment may have facilitated transport of Ni. Spinel in the Ni-harzburgite has the lowest V_2O_3 contents of the cratonic samples (Fig. 6B,C), and V becomes markedly less compatible at fO_2 > FMQ-1, and incompatible at fO_2 = FMQ (the fayalite-magnetite-quartz buffer) in both spinel and chromite (Mallmann and O'Neill, 2009). This is consistent with fO_2 ~ NNO (the Ni-Ni oxide buffer; ~ FMQ+1) indicated by equilibrium between native Ni and Ni-rich olivine (Giuliani et al., 2013a). High fO_2 would also explain the higher $Fe^{3+}/\Sigma Fe$ in Ni-rich spinel compared to spinel in symplectites not associated with Ni-rich minerals within the Ni-harzburgite (Giuliani et al., 2013a). In summary, the formation conditions in the mantle were probably near-neutral with respect to pH, with relatively high fO_2 but low fS_2.

6.4.2. Constraints from siderophile and chalcophile elements

Native Ni is generally IPGE-Rh-rich and Pt-Pd-poor, mimicking the PGE patterns of Bultfontein peridotites and, with the exception of Pd, sulphides in southern African peridotite xenoliths (Fig. 9B). Such patterns reflect those expected for depleted mantle xenoliths in general (e.g., Pearson et al., 2004) and the harzburgitic host in particular. This sample has the lowest bulk S concentration of those investigated, and one of the lowest measured in southern African peridotite xenoliths (Fig. 8A). It seems unlikely that a Ni-rich, S-poor metasomatic agent resulted from prior fractionation of mss from a sulphide melt deeper in the lithospheric column because IPGE and Rh would be removed with

this sulphide (e.g., Ballhaus et al., 2001; Liu and Brenan, 2015). The enrichment of Rh together with the observed high IPGE/Pt signature (Fig. 9B), also preclude a process involving physical entrainment, assimilation or overprinting of IPGE alloys (Lorand et al., 2013). In contrast, during partial melting, Rh concentrates in residual mss along with the IPGE, whereas Pt and Pd are highly incompatible (e.g., Ballhaus et al., 2001; Liu and Brenan, 2015). The desulphurisation of this residual mss by the metasomatic agent could then lead to alloy formation (Fonseca et al., 2012).

Djerfisherite in mantle xenoliths is thought to be related to K-Cl-bearing melts or fluids (Abersteiner et al., 2019). The small amount of djerfisherite precipitated in the Ni-enriched zone has some of the highest Pb, Ag, Se, Te and Bi abundances of all sulphides in this study (Fig. 9B), indicating efficient mobilisation of these elements in the metasomatic melt, with limited partitioning into native Ni, which has Se and Te <LOD.

6.4.3. Local replacement of sulphide residual from melt extraction

The following observations suggest that the Ni-enriched zone reflects a localised process involving desulphurisation of residual BMS phases, element redistribution and transport of Ni and Fe in the small-volume melt.

(1) Strong diffusive enrichment of Ni and Fe in silicates and spinels indicates that appreciable amounts of Ni ± Fe must have been transported in the volatile-rich melt at least at the cm to dm scale, giving rise to a Ni-enriched zone. Similarly, formation of native Ni and sulphide phases with very low PGE contents (<1 ppm total PGE abundance; Appendix 3), typical of metasomatic sulphides in this study, suggests limited transport of HSE in the metasomatic agent. In the crust, there is evidence that only Cu and Au are mobilised at km scales during greenschist-faces hydration and carbonation, whereas Ni and PGE are only mobile over a few mm (Le Vaillant et al., 2015a). Although highly saline metamorphic fluids are rich in ligands that are able to mobilise a range of ore-forming metals (Morrissey and Tomkins, 2020), it is unclear whether processes occurring during crustal metamorphism are relevant to native Ni formation in the mantle. Even when Ni-PGE geochemical halos are observed around sulphide ore deposits, As-rich hydrothermal fluids appear to be the main agent (Le Vaillant et al., 2015b), but As abundances in native Ni or djerfisherite are low (Fig. 7A,B), and their enrichment in heazlewoodite, which formed after native Ni, is here ascribed to addition during later sulphidation.
(2) Absolute HSE abundances and PM-normalised patterns in both native Ni and heazlewoodite, which partially replaced native Ni (based on textural observations; Fig. 2G), vary by several orders of magnitude (Fig. 7A,B). Such variations in the PGE content of sulphides in residual mantle peridotites may result from pre-concentration into a decreasing sulphide pool during partial melt extraction, and partial preservation if subsequently entrapped by another mineral (cf. IPGE-Rh enriched patterns of included sulphides in Alard et al., 2000).
(3) The Ni-enriched harzburgite has bulk-rock Ni abundances (1720 ppm) similar to those in the other samples in this study, which do not feature Ni-enriched zones (1120 to 1890 ppm; values from Holwell et al., 2019).
(4) Ni-enriched zones are very rarely reported in cratonic mantle xenoliths (Lorand and Grégoire, 2006), despite a plethora of studies with evidence for multiple metasomatic overprints by a variety of agents; this suggests a limited role for large-scale Ni mobility.

In light of these observations, the most plausible explanation appears to be formation of native Ni from pre-existing BMS under extremely low fS_2 imposed by the metasomatic agent in the mantle. The PGE pattern of native Ni is strikingly similar to metal-rich mss in a spinel harzburgite from Kerguelen (Fig. 7A), which experienced partial desulfidation driven by partitioning of S as well as volatile siderophile and chalcophile elements into volatile-rich fluids exsolved from carbonated silicate melt (Delpech et al., 2012). A similar process may have acted upon the Ni-mineralised sample. Silicate and oxide minerals in the Ni-enriched zones have higher FeO contents than in the unenriched parts of the harzburgite xenolith (Giuliani et al., 2013a). Thus, BMS breakdown is envisaged as a process involving replacement of S with Ni ± Fe to form native Ni (with 1.25 to 13.8 wt% Fe; Giuliani et al., 2013a), and repartitioning of excess Fe into spinel and the silicates, with small-scale transport of Fe in the metasomatic agent. As discussed by Campbell and Roeder (1968), desulphurisation entails redistribution of Ni among silicate, oxide and metal, whereby Ni uptake in olivine and pyroxene may occur via the reactions $2Ni + SiO_2 + O_2 = Ni_2SiO_4$ and $Ni + SiO_2 + ½\ O_2 = NiSiO_3$, respectively. Loss of orthopyroxene (via conversion to clinopyroxene) from the Ni-enriched assemblage would have provided a source of SiO_2. These reactions accord with the suggested increase in fO_2 during Ni enrichment and the observation that orthopyroxene is absent from the Ni-enriched part.

6.5. Resulphidation of the lithosphere beneath Bultfontein and elsewhere in the Kaapvaal craton

6.5.1. Evidence for resulphidation

Massive resulphidation of the lithospheric mantle beneath several localities in the Kaapvaal Craton after its stabilisation in the Archaean is predicated on the following observations:

(1) Although an origin from kimberlite contamination cannot be discounted (Griffin et al., 2014a; Lorand et al., 2013; Lorand and Grégoire, 2006), most peridotite xenoliths from the Kaapvaal Craton have S concentrations that are higher than expected for the degree of depletion estimated from their Al_2O_3 contents, including in the studied samples (Fig. 8A). This is particularly true given evidence for ~50% melt extraction in a harzburgite xenolith from Bultfontein, suggesting that all sulphide is of metasomatic origin (Wainwright et al., 2016).
(2) Re-Os model ages of sulphide grains in peridotite xenoliths cluster around 2.7 Ga, 2.2 to 1.8 Ga and 1.0 Ga, which suggests sulphide precipitation from asthenosphere-derived silicate melts that are introduced episodically (Griffin et al., 2003).
(3) Polymict breccias, which represent failed kimberlite intrusions (Giuliani et al., 2014a; Lawless et al., 1979; Pokhilenko, 2009), contain large (up to 2.0×0.5 cm) segregations of Fe-Ni-Cu sulphides as part of large lenses and veins of ilmenite and rutile (Giuliani et al., 2013b, 2016b). Thus, these proto-kimberlites have reached sulphide saturation at 3.0 to 3.8 GPa, where polymict breccias last equilibrated.
(4) Pentlandite in phl-peridotites is closely associated with other metasomatic phases (clinopyroxene and phlogopite), suggesting co-precipitation from a metasomatic agent.
(5) Sulphidation in the Ni-enriched harzburgite XM1/422 is evidenced by heazlewoodite overgrowths on native Ni (Fig. 2G and Giuliani et al., 2013a). The S-bearing agent also had high concentrations of As, Sb, Bi, causing the strong observed enrichment in (inclusion-free) heazlewoodite, from which gersdorffite later exsolved.
(6) Metasomatic introduction of S has been recognised in eclogite xenoliths (Burness et al., 2020; Gréau et al., 2013) that occur interspersed as pods and lenses in the regional cratonic lithospheric mantle.

Sulfidation, coupled with the observed desulfidation leading to native Ni formation discussed above, appears to be characteristic of metasomatism by volatile-rich, strongly alkaline melts, such as beneath Kerguelen (Lorand et al., 2004, Delpech et al., 2012) and the Massif

Central (Alard et al., 2011), which are also implicated in the late metasomatic enrichment in the present study.

6.5.2. Effects on siderophile and chalcophile elements

After partial melt extraction during lithosphere stabilisation, the residual mantle is expected to be IPGE-rich, and Pd- and Re-poor, with complementary depletions and enrichments in the melt (e.g., Pearson et al., 2004). The behaviour of Rh and Pt depends on the preservation of residual sulphide and stabilisation of Pt alloys, respectively (e.g., Luguet et al., 2007; Mungall and Brenan, 2014). The abundances of Re and, in particular, Pt and Os in sulphides from the strongly metasomatised peridotite xenoliths studied herein are orders of magnitude lower than those of the vast majority of BMS grains in variably depleted to mildly metasomatised peridotites from the Kaapvaal Craton (Fig. 11A,B). In fact, Pt and Os abundances extend to lower values than those of eclogitic sulphides. This is ascribed to massive dilution of the HSE content by influx of an S-rich but IPGE- and Pt-poor agent. Despite near primitive Pd/Ir-ratios in pentlandite in six of the seven samples investigated in this study (Fig. 11C), the bulk rocks in the three phlogopite-peridotites where data are available retain depleted HSE systematics with high IPGE/Pd (Fig. 7C,D). The dilution hypothesis is consistent with markedly lower bulk-rock IPGE abundances in MARID xenoliths, which can be considered more strongly metasomatised than the phl-peridotites in this study or other Bultfontein xenoliths (Fig. 9B). In contrast, the Ni-enriched harzburgite has experienced the least S addition, judging by its low bulk S abundances: ~50 ppm compared to 85 to 200 ppm in the other xenoliths (Holwell et al., 2019) and to 62–220 ppm in other peridotites from Bultfontein and nearby localities (Lorand and Grégoire, 2006).

Abundances of Zn, Ag, Cd, Te and Pb are higher in phl-peridotites and MARID than in polymict breccias, with As, Sb, Ag, Te and Pb conspicuously higher in the MARID pentlandite (Fig. 5). Therefore, from a chalcophile-element perspective, the Ti-rich silicate melts that metasomatised the phl-peridotites coeval with Karoo magmatism (Giuliani et al., 2014b; Appendix 1) appear to be related to the metasomatic agent responsible for MARID formation. These melts caused stronger HSE dilution but greater addition of the chalcogens and some chalcophile elements. A similar genetic relationship between MARID and phlogopite-rich peridotites has been proposed based on Sr isotope and trace-element ratios in clinopyroxene (Fitzpayne et al., 2020). In contrast, sulphides in the polymict breccias are generally poorer in chalcophile elements, suggesting that the proto-kimberlite melts engulfing the mixtures of mantle-derived porphyroclasts that make up the polymict breccias (Giuliani et al., 2014a; Lawless et al., 1979; Pokhilenko, 2009) had higher ratios of S to chalcophile elements than the silicate melts (Figs. 5 and 7).

It is striking that pentlandite in five of the seven samples discussed here has markedly supra-PUM Ru/Ir. This is also true for coexisting chalcopyrite in two of the samples (Fig. 7E–F) and therefore is not an artefact of an unrecognised NiAr interference. Although bulk-rock data are not available for MARID sample BLFX-3, one of the two MARID rocks from Bultfontein analysed by Maier et al. (2012) has similarly high Ru/Ir; this signature is shared by the majority of metasomatic BMS in eclogite xenoliths (Burness et al., 2020; Fig. 11C). Elevated Ru/Ir may be a hallmark of sulphides in strongly metasomatised peridotites from the Kaapvaal Craton, whereas this signature is barely expressed at the bulk-rock scale. It is also recognised in peridotites from the Western Gneiss Region in Norway (Fig. 11C), which were metasomatised by hydrous melts and fluids generated in subduction zones, and is a signature of Cu ± Au deposits (Rielli et al., 2018a), although these samples range to much higher Pd/Ir. In addition, the strongly metasomatised peridotites targeted in this study have high Te abundances (from Holwell et al., 2019) at a given S content compared to literature values. These concentrations are more similar to those of eclogite xenoliths than to other peridotite xenoliths from the Kaapvaal Craton (Fig. 8B,C), consistent with metasomatic modification and formation of Pt-Pd-Te phases, which have also been identified in other mantle rocks (e.g., König et al., 2014).

6.5.3. A role for subducted components

Depletion of the compatible IPGE and enrichment in incompatible Pd would be characteristic of any melt, but is tentatively ascribed here to sourcing of the metasomatic agents in mantle domains containing subducted components, given i) evidence for non-mantle S, N and O isotope compositions (Giuliani et al., 2016a; Fitzpayne et al., 2019a); ii) the Ni-poor character of sulphides in Kaapvaal peridotite xenoliths, inconsistent with equilibrium with peridotitic mantle (Lorand and Grégoire, 2006); and iii) young ages and radiogenic initial Os isotopic compositions in peridotitic sulphide inclusions in diamond, which have been explained by remobilisation of older eclogitic components (Aulbach et al., 2009a, 2009b). Two sulphidation mechanisms were identified in prior works: (i) immiscibility of Cu-Ni rich sulfide melt droplets, which unmix from the carbonate melt fraction, with precipitation of IPGE-rich, PPGE poor mss and Pt-bismuthotellurides; (ii) sulfidation reactions from an S-H-CO_2-rich supercritical fluid that introduced S, Pd, Os, As and some Au (Lorand et al., 2004; Alard et al., 2000; Delpech et al., 2012). In view of the above-described siderophile and chalcophile element systematics, strongly metasomatised Bultfontein peridotites and MARID rocks are suggested to have interacted with a volatile-rich fluid at least partly sourced from subducted components.

6.6. Implications of resulphidation for the formation of PGE deposits

This study shows that the resulphidation of the Kaapvaal lithospheric mantle after its initial depletion led to a dilution of PGE, perhaps formerly hosted in PGM or rare sulphide inclusions, into larger volumes of sulphide. The bulk-rock IPGE abundances remain largely similar to PM (Fig. 9B), suggesting that the low HSE contents in the sulphides are offset by their increased modal abundances. Based on the analysis of PGE contents in kimberlites, which represent the sum of kimberlite melt contribution plus entrained and digested mantle xenoliths, Maier et al. (2017) suggested that the SCLM does not significantly contribute to the PGE enrichment associated with large igneous provinces. However, in the whole-rock peridotites and the BMS studied here, Au_{PUM} is high relative to the less incompatible (during mantle melting) Pd_{PUM} compared to BMS in other Kaapvaal peridotite xenoliths (Fig. 9B). Indeed, the average bulk-sample Au abundance in non-MARID metasomatised peridotites from Bultfontein is 1.9 ± 1.9 ppb (n = 12), while that in MARID is similarly high but less variable (1.9 ± 0.8 ppb, n = 6); for comparison, only 1.0 ± 1.0 ppb (n = 52) Au has been measured in the remaining southern African localities (data in Maier et al., 2012; Holwell et al., 2019). This suggests that strong metasomatism, such as that recorded beneath Bultfontein can replenish at least some of the Au in parts of the lithospheric mantle.

Remobilisation of HSE from the shallow cratonic mantle lithosphere, where temperatures are below those leading to incongruent melting of mss (Ballhaus et al., 2006) probably requires oxidation to sulphate, at fO_2 > FMQ (Jugo, 2009), or dissolution of sulphides. Although sulphate-bearing veins occur in MARID rocks from Bultfontein (Giuliani et al., 2014b), consistent with the presence of localised and perhaps transient oxidised domains in the mantle lithosphere, fO_2 largely remains <FMQ even in shallow metasomatised mantle xenoliths from the Kaapvaal Craton (Woodland and Koch, 2003). Thus, S must be remobilised in sulphide-undersaturated melts, such as ascending silicate melts, in which S concentrations at sulphide saturation (SCSS) increase with decreasing pressure and increasing fO_2 (e.g., Mavrogenes and O'Neill, 1999) also depending on melt SiO_2 (Chowdhury and Dasgupta, 2020) and FeO (Wykes et al., 2015).

We envisage that the resulphidation of initially refractory cratonic lithospheric mantle occurred over aeons, as constrained from sulphide Re-Os dating (e.g. at 2.2 to 1.8 Ga; Griffin et al., 2004), and was accompanied by re-introduction of PGE. These early metasomatic sulphides

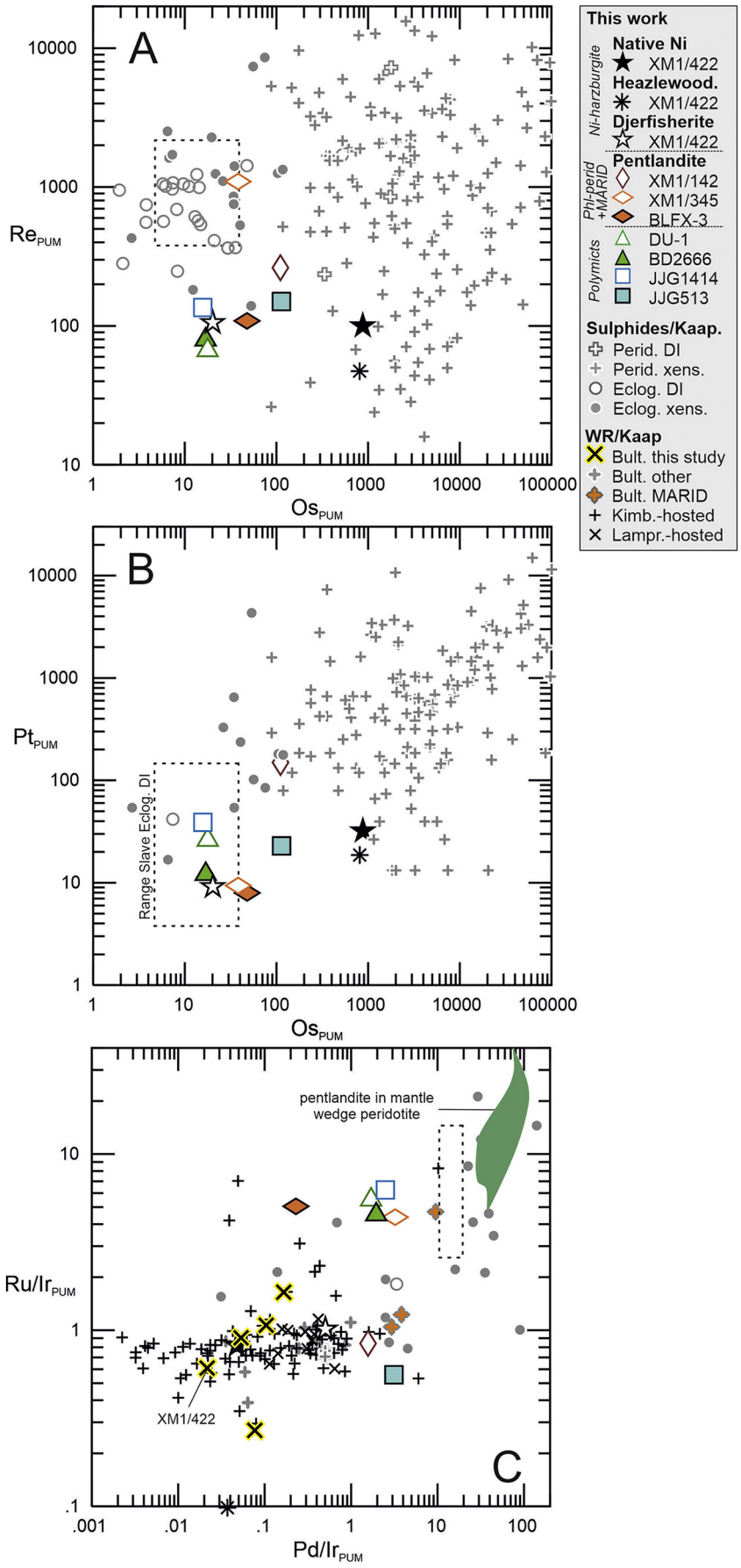
A
B
C
Re$_{PUM}$
Os$_{PUM}$
Pt$_{PUM}$
Ru/Ir$_{PUM}$
Pd/Ir$_{PUM}$
Range Slave Eclog. DI
pentlandite in mantle wedge peridotite
XM1/422
This work
Native Ni
XM1/422
Heazlewood.
XM1/422
Djerfisherite
XM1/422
Ni-harzburgite
Pentlandite
XM1/142
XM1/345
BLFX-3
Phl-perid +MARID
DU-1
BD2666
JJG1414
JJG513
Polymicts
Sulphides/Kaap.
Perid. DI
Perid. xens.
Eclog. DI
Eclog. xens.
WR/Kaap
Bult. this study
Bult. other
Bult. MARID
Kimb.-hosted
Lampr.-hosted

may have been in part dissolved into the large-volume melt that led to formation of the massive ca. 2.05 Ga Bushveld layered intrusion, which contains the largest PGE reserves on the planet. Indeed, a role of the continental lithospheric mantle in the genesis of the Bushveld magmas has been proposed (e.g. Richardson and Shirey, 2008). Small-volume carbonated melts percolated the lithosphere at least from the Palaeoproterozoic onwards, as exemplified by the ca. 1.8 to 1.6 Ga Kuruman kimberlite province (Donnelly et al., 2012), the ca. 1.15–1.13 Ga Premier (Cullinan) kimberlite (Tappe et al., 2018), and the Jurassic and Cretaceous lamproite/orangeite and kimberlite magmatism, respectively (e.g., Griffin et al., 2014a).

The repeated percolation of Ti-enriched silicate melts (phl-peridotites, MARID) and small-volume carbonated melts (polymict breccias) caused both net addition and intra-lithospheric redistribution of S previously stored deeper in the lithosphere, including in subducted materials. A similar remobilisation model of earlier-emplaced subducted components has been proposed for the generation of Cu-Au deposits, which have elevated Ru/Ir, similar to the Bultfontein samples (Rielli et al., 2018a). Gold and some chalcophile elements would follow S and partition into the newly-formed sulphide. This may represent a first step in the focussing and pre-concentration of precious metals into sulphides at increasingly shallower depth.

7. Summary and conclusions

We have investigated the petrography and chemical composition of native Ni, sulphide, spinel and Ti-oxide phases in a suite of well-characterised, highly metasomatised peridotites from the Bultfontein kimberlite (Kaapvaal Craton) in order to (1) constrain to which extent these macroscopic minerals control the chalcophile and siderophile budget in the cratonic lithospheric mantle, (2) assess the effects of low-temperature processes on late-stage remobilisation and redistribution of these elements, (3) decipher the nature and effects of metasomatic processes acting on the mineralogical hosts of siderophile and chalcophile elements at mantle depth, and (4) discuss implications for first-order controls for enhanced lithospheric mantle fertility. Our main conclusions are as follows:

- Spinels host an insignificant proportion of the siderophile and chalcophile elements, except Zn. Despite orders of magnitude higher abundances of most chalcophile and siderophile elements in the investigated macroscopic BMS and native Ni, these phases account for only a small proportion of the bulk-rock PGE or Au budget (typically <25%), and additional hosts are required. One Pt-Au micro-nugget was directly observed, whereas micro-nuggets with or without semimetals are indirectly observed in time-resolved LAM-ICPMS spectra. High bulk-rock Te/S ratios suggest a role for tellurides, which along with bismuthinides, antimonides and similar compounds may also host missing As, Ag, Cd, Sb, Te and in part Bi. Combined with low Se/Te, this indicates the introduction of chalcophile and chalcogen elements via metasomatism.
- Low-temperature re-equilibration of monosulfide solid solution to pentlandite + pyrrhotite + chalcopyrite entails limited redistribution of chalcophile and siderophile elements, with slightly higher PGE abundances in pentlandite, which therefore yields maximum concentrations relative to the bulk sulphide. Serpentinisation may not have been isochemical with respect to chalcophile and siderophile elements, as heazlewoodite replacing "primary" pentlandite has consistently higher As, Ag, Sb, Te, Bi, Pb and Au, perhaps pointing to the efficient transport of chalcophile elements and Au in the serpentinising agent. Conversely, the mobility of PGE at the mineral scale appears to be negligible during serpentinisation.
- Multiple pieces of evidence in this and prior work indicate that after its formation and strong melt depletion, the Kaapvaal Craton has experienced repeated sulphide addition due to multiple metasomatic events. At Bultfontein, this caused massive dilution of HSE abundances in pre-existing PGM and residual sulphides, with formation of markedly PGE-poor BMS (<4.2 ppm total PGE contents in pentlandite from seven samples), compared to >26 ppm in BMS in other Kaapvaal peridotite xenoliths. In the metasomatised bulk peridotites, Au is enriched relative to the less incompatible Pd and was probably added along with S, possibly partly sourced from subducted materials. Conversely, native Ni, which occurs in unusual Ni-enriched zones in a harzburgite, probably formed from precursor BMS due to strong desulphurisation.
- Episodic sulphide formation in strongly metasomatised peridotite at mid-lithospheric depths possibly involved a combination of net introduction of S and HSE during interaction with asthenosphere-derived silicate melts, and intra-lithospheric redistribution during metasomatism by small-volume carbonated melts. Such upward redistribution may represent an important step in the pre-concentration of precious metals in the lithospheric mantle. Further mobilisation may be promoted where these metal-enriched sulphide-bearing domains in the mantle interact with ascending sulphide-undersaturated melts. These processes would ultimately represent the first-order controls on the prospectivity of any given overlying crustal block.

Declaration of Competing Interest

The authors declare that they have no known competing financial interests or personal relationships that could have appeared to influence the work reported in this paper.

Acknowledgements

We would like to thank Graham Hutchinson for support with the EMP analyses at the University of Melbourne, and Bruce Wyatt and the De Beers Group for providing access to the studied samples. Comments by Andy Tomkins and an anonymous reviewer significantly improved the manuscript, for which we are sincerely grateful. MF acknowledges the financial support of the Australian Research Council (ARC), Australia through funding from the Centre of Excellence for Core to Crust Fluid Systems (CE110001017), ARC Linkage Project LP120100668 and the Future Fellowship Scheme (FT110100241). VSK was supported by the Russian Science Foundation, Russia grant 16-17-10145. This is contribution 1540 from the ARC Centre of Excellence for Core to Crust Fluid Systems (http://www.ccfs.mq.edu.au) and 1480 in the GEMOC Key Centre (http://www.gemoc.mq.edu.au). The analytical data were obtained using instrumentation funded by DEST Systemic Infrastructure Grants, ARC LIEF, NCRIS/AuScope, industry partners and Macquarie University.

Fig. 11. Trace-element abundances (ppm) and primitive mantle-normalised ratios in native Ni and pentlandite in Ni-enriched harzburgite, phlogopite-rich peridotites, MARID and polymict breccia xenoliths from Bultfontein. Primitive mantle values from Becker et al. (2006) and Fischer-Gödde et al. (2011), with the following values and uncertainties: Os = 3.9 ± 0.5 ppb, Ir = 3.5 ± 0.4 ppb, Ru = 7.0 ± 0.9 ppb, Pt = 7.6 ± 1.3 ppb, Pd = 7.1 ± 1.3 ppb, Re = 0.35 ± 0.06 ppb. Shown for comparison are various samples from southern Africa, including mss in peridotite (Alard et al., 2000) and in eclogite xenoliths (Burness et al., 2020), sulphide inclusions in peridotitic and eclogitic diamond (Pearson et al., 1998; Richardson et al., 2001; Richardson et al., 2004; Aulbach et al., 2009b), whole-rock peridotite xenoliths from Bultfontein investigated in this study (data from Holwell et al., 2019) and in prior work (Maier et al., 2012) as well other kimberlite- and lamproite-hosted peridotite xenoliths (Pearson et al., 2004; Maier et al., 2012) from southern Africa. Field in C. shows pentlandite in peridotite from the Western Gneiss Region in Norway representing an exhumed mantle wedge (Rielli et al., 2018a); dashed box in all panels encompasses maximum and minimum concentrations in sulphide inclusions in eclogitic diamond from the central Slave craton, interpreted to represent oceanic crust that was affected only by subduction processes, i.e. unmetasomatised (Aulbach et al., 2012).

Appendix A. Supplementary data

Supplementary data to this article can be found online at https://doi.org/10.1016/j.lithos.2020.105880.

References

Abersteiner, A., Kamenetsky, V.S., Goemann, K., Golovin, A.V., Sharygin, I.S., Giuliani, A., Rodemann, T., Spetsius, Z.V., Kamenetsky, M., 2019. Djerfisherite in kimberlites and their xenoliths: implications for kimberlite melt evolution. Contrib. Mineral. Petrol. 174.

Alard, O., Griffin, W.L., Lorand, J.P., Jackson, S.E., O'Reilly, S.Y., 2000. Non-chondritic distribution of the highly siderophile elements in mantle sulphides. Nature 407, 891–894.

Alard, O., Lorand, J.P., Reisberg, L., Bodinier, J.L., Dautria, J.M., O'Reilly, S.Y., 2011. Volatile-rich Metasomatism in Montferrier Xenoliths (Southern France): Implications for the Abundances of Chalcophile and Highly Siderophile Elements in the Subcontinental Mantle. J. Petrol. 52, 2009–2045.

Arguin, J.P., Page, P., Barnes, S.J., Yu, S.Y., Song, X.Y., 2016. The effect of chromite crystallization on the distribution of osmium, iridium, ruthenium and rhodium in picritic magmas: an example from the emeishan large igneous Province, Southwestern China. J. Petrol. 57, 1019–1047.

Arndt, N.T., 2013. The lithospheric mantle plays no active role in the formation of orthomagmatic Ore deposits. Econ. Geol. 8, 1953–1970.

Aulbach, S., Shirey, S.B., Stachel, T., Creighton, S., Muehlenbachs, K., Harris, J.W., 2009a. Diamond formation episodes at the southern margin of the Kaapvaal Craton: Re-Os systematics of sulfide inclusions from the Jagersfontein Mine. Contrib. Mineral. Petrol. 157, 525–540.

Aulbach, S., Stachel, T., Creaser, R.A., Heaman, L.M., Shirey, S.B., Muehlenbachs, K., Eichenberg, D., Harris, J.W., 2009b. Sulphide survival and diamond genesis during formation and evolution of Archaean subcontinental lithosphere: a comparison between the Slave and Kaapvaal cratons. Lithos 112, 747–757.

Aulbach, S., Stachel, T., Seitz, H.-M., Brey, G.P., 2012. Chalcophile and siderophile elements in sulphide inclusions in eclogitic diamonds and metal cycling in a Paleoproterozoic subduction zone. Geochim. Cosmochim. Acta 93, 278–299.

Aulbach, S., Mungall, J.E., Pearson, D.G., 2016. Distribution and processing of highly siderophile elements in cratonic mantle lithosphere. Highly siderophile and strongly chalcophile elements in high-temperature. Geochem. Cosmochem. 81, 239–304.

Aulbach, S., Sun, J., Tappe, S., Höfer, H.E., Gerdes, A., 2017. Volatile-rich metasomatism in the cratonic mantle beneath SW Greenland: link to Kimberlites and Mid-lithospheric discontinuities. J. Petrol. 58, 2311–2338.

Aulbach, S., Sun, J., Tappe, S., Gerdes, A., 2019. Effects of multi-stage rifting and metasomatism on HSE-Os-187/Os-188 systematics of the cratonic mantle beneath SW Greenland. Contrib. Mineral. Petrol. 174.

Ballhaus, C., 1995. Is the upper mantle metal-saturated? Earth Planet. Sci. Lett. 132, 75–86.

Ballhaus, C., Berry, R., Green, D., 1991. High pressure experimental calibration of the olivine-orthopyroxene-spinel oxygen geobarometer: implications for the oxidation state of the upper mantle. Contrib. Mineral. Petrol. 107, 27–40.

Ballhaus, C., Tredoux, M., Spath, A., 2001. Phase relations in the Fe-Ni-Cu-PGE-S system at magmatic temperature and application to massive sulphide ores of the Sudbury Igneous Complex. J. Petrol. 42, 1911–1926.

Ballhaus, C., Bockrath, C., Wohlgemuth-Ueberwasser, C., Laurenz, V., Berndt, J., 2006. Fractionation of the noble metals by physical processes. Contrib. Mineral. Petrol. 152, 667–684.

Barnes, S.J., 2016. Chalcophile elements. In: White, W.M. (Ed.), Encyclopedia of Geochemistry. Springer, Cham, pp. 1–5.

Barnes, S.J., Liu, W., 2012. Pt and Pd mobility in hydrothermal fluids: evidence from komatiites and from thermodynamic modelling. Ore Geol. Rev. 44, 49–58.

Baumgartner, R.J., Fiorentini, M.L., Baratoux, D., Ferriere, L., Locmelis, M., Tomkins, A., Sener, K.A., 2017. The variability of ruthenium in chromite from chassignite and olivine-phyric shergottite meteorites: new insights into the behavior of PGE and sulfur in Martian magmatic systems. Meteorit. Planet. Sci. 52, 233–350.

Becker, H., Horan, M.F., Walker, R.J., Gao, S., Lorand, J.-P., Rudnick, R.L., 2006. Highly siderophile element composition of the Earth's primitive upper mantle: constraints from new data on peridotite massifs and xenoliths. Geochim. Cosmochim. Acta 70, 4528–4550.

Bell, D.R., Rossman, G.R., Moore, R.O., 2004. Abundance and partitioning of OH in a high-pressure magmatic system: megacrysts from the Monastery kimberlite, South Africa. J. Petrol. 45, 1539–1564.

Bell, D.R., Gregoire, M., Grove, T.L., Chatterjee, N., Carlson, R.W., Buseck, P.R., 2005. Silica and volatile-element metasomatism of Archean mantle: a xenolith-scale example from the Kaapvaal Craton. Contrib. Mineral. Petrol. 150, 251–267.

Bragagni, A., Luguet, A., Fonseca, R.O.C., Pearson, D.G., Lorand, J.P., Nowell, G.M., Kjarsgaard, B.A., 2017. The geological record of base metal sulfides in the cratonic mantle: a microscale Os-187/Os-188 study of peridotite xenoliths from Somerset Island, Rae Craton (Canada). Geochim. Cosmochim. Acta 216, 264–285.

Brenan, J.M., Finnigan, C.F., McDonough, W.F., Homolova, V., 2012. Experimental constraints on the partitioning of Ru, Rh, Ir, Pt and Pd between chromite and silicate melt: the importance of ferric iron. Chem. Geol. 302, 16–32.

Brey, G.P., Köhler, T., Nickel, K.G., 1990. Geothermobarometry in 4-phase lherzolites. 1. Experimental results from 10 to 60 KB. J. Petrol. 31, 1313–1352.

Buick, I.S., Maas, R., Gibson, R., 2001. Precise U-Pb titanite age constraints on the emplacement of the Bushveld complex. S. Afr. J. Geol. 158, 3–6.

Burness, S., Smart, K.A., Tappe, S., Stevens, G., Woodland, A.B., Cano, E., 2020. Sulphur-rich mantle metasomatism of Kaapvaal craton eclogites and its role in redox-controlled platinum group element mobility. Chem. Geol. 119476 In press.

Campbell, A.J., Roeder, P., 1968. The stability of olivine and pyroxene in the Ni-Mg-Si-O system. Am. Mineral. 53, 257–268.

Choi, E., Fiorentini, M.L., Hughes, H.S.R., Giuliani, A., 2020. Platinum-group element and Au geochemistry of Late Archean to Proterozoic talc-alkaline and alkaline magmas in the Yilgarn Craton, Western Australia. Lithos 374.

Chowdhury, P., Dasgupta, R., 2020. Sulfur extraction via carbonated melts from sulfide-bearing mantle lithologies – implications for deep sulfur cycle and mantle redox. Geochim. Cosmochim. Acta 269, 376–397.

Cornell, D.H., Armstrong, R.A., Walraven, F., 1998. Geochronology of the Proterozoic Hartley Basalt Formation, South Africa: constraints on the Kheis tectogenesis and the Kaapvaal Craton's earliest Wilson Cycle. J. Afr. Sci. 26, 5–27.

Dare, S.A.S., Barnes, S.-J., Beaudoin, G., 2012. Variation in trace element content of magnetite crystallized from a fractionating sulfide liquid, Sudbury, Canada: implications for provenance discrimination. Geochim. Cosmochim. Acta 88, 27–50.

Dawson, J.B., Smith, J.V., 1977. MARID (mica-amphibole-rutile-ilmenite-diopside) suite of xenoliths in kimberlite. Geochim. Cosmochim. Acta 41, 309–323.

De Wit, M., Thiart, C., 2005. Metallogenic fingerprints of Archaean cratons. Min. Depos. Earth Evol. 248, 59–70.

de Wit, M.J., Roering, C., Hart, R.J., Armstrong, R.A., de Ronde, C.E.J., Green, R.W.E., Tredoux, M., Peberdy, E., Hart, R.A., 1992. Formation of an Archaean continent. Nature 357, 553–562.

Delpech, G., Lorand, J.P., Gregoire, M., Cottin, J.Y., O'Reilly, S.Y., 2012. In-situ geochemistry of sulfides in highly metasomatized mantle xenoliths from Kerguelen, southern Indian Ocean. Lithos 154, 296–314.

Donnelly, C.L., Griffin, W.L., Yang, J.-H., O'Reilly, S.Y., Li, Q.-L., Pearson, N.J., Li, X.-H., 2012. In situ U^Pb Dating and Sr^Nd isotopic analysis of perovskite: constraints on the Age and Petrogenesis of the Kuruman Kimberlite Province, Kaapvaal Craton, South Africa. J. Petrol. 53, 2497–2522.

Duncan, R.A., Hooper, P.R., Rehacek, J., Marsh, J.S., Duncan, A.R., 1997. The timing and duration of the Karoo igneous event, southern Gondwana. J. Geophys. Res. 102, 18127–18138.

Eldridge, C.S., Compston, W., Williams, I.S., Harris, J.W., Bristow, J.W., 1991. Isotope evidence for the involvement of recycled sedeiments in diamond formation. Nature 353, 649–653.

Erlank, A.J., Waters, F.G., Hawkesworth, C.J., Haggerty, S.E., Rickard, R.S., Menzies, M., 1987. Evidence for mantle metasomatism in peridotite nodules from the Kimberley pipes, South Africa. In: Menzies, M., Hawkesworth, C.J. (Eds.), Mantle Metasomatism. Academic Press, London, pp. 221–312.

Ferraris, C., Lorand, J.P., 2008. HRTEM-AEM-HAADF-STEM study of platinum-group elements within a mantle-derived Cr spinet (Lherz; North-Eastern Pyrenees, France). Earth Planet. Sci. Lett. 276, 167–174.

Ferraris, C., Lorand, J.P., 2015. Novodneprite (AuPb3), anyuiite Au(Pb, Sb)(2) and gold micro- and nano-inclusions within plastically deformed mantle-derived olivine from the Lherz peridotite (Pyrenees, France): a HRTEM-AEM-EELS study. Phys. Chem. Miner. 42, 143–150.

Field, M., Stiefenhofer, J., Robey, J., Kurszlaukis, S., 2008. Kimberlite-hosted diamond deposits of Southern Africa: a review. Ore Geol. Rev. 34, 33–75.

Finnigan, C.S., Brenan, J.M., Mungall, J.E., McDonough, W.F., 2008. Experiments and models bearing on the role of chromite as a collector of platinum group minerals by local reduction. J. Petrol. 49, 1647–1665.

Fiorentini, M.L., Stone, W.E., Beresford, S.W., Barley, M.E., 2004. Platinum-group element alloy inclusions in chromites from Archaean mafic-ultramafic units: evidence from the Abitibi and the Agnew-Wiluna Greenstone Belts. Mineral. Petrol. 82, 341–355.

Fischer-Gödde, M., Becker, H., Wombacher, F., 2011. Rhodium, gold and other highly siderophile elements in orogenic peridotites and peridotite xenoliths. Chem. Geol. 280, 365–383.

Fitzpayne, A., Giuliani, A., Hergt, J., Phillips, D., Janney, P., 2018. New geochemical constraints on the origins of MARID and PIC rocks: implications for mantle metasomatism and mantle-derived potassic magmatism. Lithos 318, 478–493.

Fitzpayne, A., Giuliani, A., Harris, C., Thomassot, E., Cheng, C., Hergt, J., 2019a. Evidence for subduction-related signatures in the southern African lithosphere from the N-O isotopic composition of metasomatic mantle minerals. Geochim. Cosmochim. Acta 266, 237–257.

Fitzpayne, A., Giuliani, A., Maas, R., Hergt, J., Janney, P., Phillips, D., 2019b. Progressive metasomatism of the mantle by kimberlite melts: Sr–Nd–Hf–Pb isotope compositions of MARID and PIC minerals. Earth Planet. Sci. Lett. 509, 15–26.

Fitzpayne, A., Giuliani, A., Hergt, J., Woodhead, J.D., Maas, R., 2020. Isotopic analyses of clinopyroxenes demonstrate the effects of kimberlite melt metasomatism upon the lithospheric mantle. Lithos 370-371, 105595.

Fleet, M.E., Liu, M.H., Crocket, J.H., 1999. Partitioning of trace amounts of highly siderophile elements in the Fe-Ni-S system and their fractionation in nature. Geochim. Cosmochim. Acta 63, 2611–2622.

Fonseca, R.O.C., Laurenz, V., Mallmann, G., Luguet, A., Hoehne, N., Jochum, K.P., 2012. New constraints on the genesis and long-term stability of Os-rich alloys in the Earth's mantle. Geochim. Cosmochim. Acta 87, 227–242.

Gervilla, F., Proenza, J.A., Frei, R., González-Jiménez, J.M., Garrido, C.J., Melgarejo, J.C., Meibom, A., Díaz-Martínez, R., Lavaut, W., 2005. Distribution of platinum-group elements and Os isotopes in chromite ores from Mayarí-Baracoa Ophiolilte Belt (eastern Cuba). Contrib. Mineral. Petrol. 150, 589–607.

Gilbert, S., Danyushevsky, L., Robinson, P., Wohlgemuth-Ueberwasser, C., Pearson, N., Savard, D., Norman, M., Hanley, J., 2013. A comparative study of five reference materials and the lombard meteorite for the determination of the platinum-group elements and gold by LA-ICP-MS. Geostand. Geoanal. Res. 37, 51–64.

Giuliani, A., Kamenetsky, V.S., Phillips, D., Kendrick, M.A., Wyatt, B.A., Goemann, K., 2012. Nature of alkali-carbonate fluids in the sub-continental lithospheric mantle. Geology 40, 967–970.
Giuliani, A., Kamenetsky, V.S., Kendrick, M.A., Phillips, D., Goemann, K., 2013a. Nickel-rich metasomatism of the lithospheric mantle by pre-kimberlitic alkali-S-Cl-rich C-O-H fluids. Contrib. Mineral. Petrol. 165, 155–171.
Giuliani, A., Kamenetsky, V.S., Kendrick, M.A., Phillips, D., Wyatt, B.A., Maas, R., 2013b. Oxide, sulphide and carbonate minerals in a mantle polymict breccia: metasomatism by proto-kimberlite magmas, and relationship to the kimberlite megacrystic suite. Chem. Geol. 353, 4–18.
Giuliani, A., Phillips, D., Kamenetsky, V.S., Kendrick, M.A., Wyatt, B.A., Goemann, K., Hutchinson, G., 2014a. Petrogenesis of mantle polymict Breccias: insights into mantle processes coeval with kimberlite magmatism. J. Petrol. 55, 831–858.
Giuliani, A., Phillips, D., Maas, R., Woodhead, J.D., Kendrick, M.A., Greig, A., Armstrong, R.A., Chew, D., Kamenetsky, V.S., Fiorentini, M.L., 2014b. LIMA U-Pb ages link lithospheric mantle metasomatism to Karoo magmatism beneath the Kimberley region, South Africa. Earth Planet. Sci. Lett. 401, 132–147.
Giuliani, A., Phillips, D., Woodhead, J.D., Kamenetsky, V.S., Fiorentini, M.L., Maas, R., Soltys, A., Armstrong, R.A., 2015. Did diamond-bearing orangeites originate from MARID-veined peridotites in the lithospheric mantle? Nat. Commun. 6, 6837.
Giuliani, A., Fiorentini, M.L., Martin, L.A.J., Farquhar, J., Phillips, D., Griffin, W.L., LaFlamme, C., 2016a. Sulfur isotope composition of metasomatised mantle xenoliths from the Bultfontein kimberlite (Kimberley, South Africa): contribution from subducted sediments and the effect of sulfide alteration on S isotope systematics. Earth Planet. Sci. Lett. 445, 114–124.
Giuliani, A., Phillips, D., Kamenetsky, V.S., Goemann, K., 2016b. Constraints on kimberlite ascent mechanisms revealed by phlogopite compositions in kimberlites and mantle xenoliths. Lithos 240, 189–201.
Giuliani, A., Soltys, A., Phillips, D., Kamenetsky, V.S., Maas, R., Goemann, K., Woodhead, J.D., Drysdale, R.N., Griffin, W.L., 2017. The final stages of kimberlite petrogenesis: petrography, mineral chemistry, melt inclusions and Sr-C-O isotope geochemistry of the Bultfontein kimberlite (Kimberley, South Africa). Chem. Geol. 455, 342–356.
Giuliani, A., Woodhead, J.D., Phillips, D., Maas, R., Davies, G.R., Griffin, W.L., 2018. Titanates of the lindsleyite-mathiasite (LIMA) group reveal isotope disequilibrium associated with metasomatism in the mantle beneath Kimberley (South Africa). Earth Planet. Sci. Lett. 482, 253–264.
González-Jiménez, J.M., Gervilla, F., Proenza, J.A., Augé, T., Kerestedjian, T., 2009. Distribution of platinum-group minerals in ophiolitic chromitites. Appl. Earth Sci. Trans. Inst. Min. Metall. B 118, 101–110.
Gréau, Y., Alard, O., Griffin, W.L., Huang, J.X., O'Reilly, S.Y., 2013. Sulfides and chalcophile elements in Roberts Victor eclogites: Unravelling a sulfide-rich metasomatic event. Chem. Geol. 354, 73–92.
Grégoire, M., Bell, D.R., Le Roex, A.P., 2002. Trace element geochemistry of phlogopite-rich mafic mantle xenoliths: their classification and their relationship to phlogopite-bearing peridotites and kimberlites revisited. Contrib. Mineral. Petrol. 142, 603–625.
Grégoire, M., Bell, D.R., Le Roex, A.P., 2003. Garnet lherzolites from the Kaapvaal craton (South Africa): trace element evidence for a metasomatic history. J. Petrol. 44, 629–657.
Griffin, W.L., Smith, D., Boyd, F.R., Cousens, D.R., Ryan, C.G., Sie, S.H., Suter, G.F., 1989. Trace-element zoning in garnets from sheared mantle xenoliths. Geochim. Cosmochim. Acta 53, 561–567.
Griffin, W.L., Spetsius, Z.V., Pearson, N.J., O'Reilly, S.Y., 2002. In situ Re-Os analysis of sulfide inclusions in kimberlitic olivine: new constraints on depletion events in the Siberian lithospheric mantle. Geochem. Geophys. Geosyst. 3.
Griffin, W.L., O'Reilly, S.Y., Natapov, L.M., Ryan, C.G., 2003. The evolution of lithospheric mantle beneath the Kalahari Craton and its margins. Lithos 71, 215–241.
Griffin, W.L., Graham, S., O'Reilly, S.Y., Pearson, N.J., 2004. Lithosphere evolution beneath the Kaapvaal Craton: Re-Os systematics of sulfides in mantle-derived peridotites. Chem. Geol. 208, 89–118.
Griffin, W.L., Begg, G.C., O'Reilly, S.Y., 2013. Continental-root control on the genesis of magmatic ore deposits. Nat. Geosci. 6, 905–910.
Griffin, W.L., Batumike, J.M., Greau, Y., Pearson, N.J., Shee, S.R., O'Reilly, S.Y., 2014a. Emplacement ages and sources of kimberlites and related rocks in southern Africa: U-Pb ages and Sr-Nd isotopes of groundmass perovskite. Contrib. Mineral. Petrol. 168, 1032.
Griffin, W.L., Pearson, N.J., Andersen, T., Jackson, S.E., O'Reilly, S.Y., Zhang, M., 2014b. Sources of cratonic metasomatic fluids: In situ LA-MC-ICPMS analysis of Sr, Nd, Hf and Pb isotopes in LIMA from the Jagersfontein kimberlite. Am. J. Sci. 314, 435–461.
Groves, D.I., Ho, S.E., Rock, N.M.S., Barley, M.E., Muggeridge, M.Y., 1987. Archaean cratons, diamond and platinum; evidence for coupled long-lived crust–mantle systems. Geology 15, 801–805.
Hanley, J.J., Pettke, T., Mungall, J.E., Spooner, E.T.C., 2005. The solubility of platinum and gold in NaCl brines at 1.5 kbar, 600 to 800 degrees C: a laser ablation ICP-MS pilot study of synthetic fluid inclusions (vol 10, pg 2593, 2005). Geochim. Cosmochim. Acta 69, 5635–5637.
Hawkesworth, C.J., Cawood, P.A., Dhuime, B., Kemp, T.I.S., 2017. Earth's continental lithosphere through time. Annu. Rev. Earth Planet. Sci. 45 (45), 169–198.
Helmy, H.M., Botcharnikov, R.E., 2020. Experimental determination of the phase relations of Pt and Pd antimonides and bismuthinides in the Fe-Ni-Cu sulfide systems between 1100 and 700C. Am. Mineral. 105, 344–352.
Helmy, H.M., Bragagni, A., 2017. Platinum-group elements fractionation by selective complexing, the Os, Ir, Ru, Rh-arsenide-sulfide systems above 1020 degrees C. Geochim. Cosmochim. Acta 216, 169–183.
Helmy, H.M., Ballhaus, C., Berndt, J., Bocrath, C., Wohlgemuth-Ueberwasser, C., 2007. Formation of Pt, Pd and Ni tellurides: experiments in sulfide-telluride systems. Contrib. Mineral. Petrol. 153, 577–591.
Helmy, H.M., Ballhaus, C., Wohlgemuth-Ueberwasser, C., Fonseca, R.O.C., Laurenz, V., 2010. Partitioning of Se, As, Sb, Te and Bi between monosulfide solid solution and sulfide melt - Application to magmatic sulfide deposits. Geochim. Cosmochim. Acta 74, 6174–6179.
Helmy, H.M., Ballhaus, C., Fonseca, R.O.C., Wirth, R., Nagel, T., Tredoux, M., 2013. Noble metal nanoclusters and nanoparticles precede mineral formation in magmatic sulphide melts. Nat. Commun. 4.
Holwell, D.A., Fiorentini, M., McDonald, I., Lu, Y., Giuliani, A., Smith, D.J., Keith, M., Locmelis, M., 2019. A metasomatized lithospheric mantle control on the metallogenic signature of post-subduction magmatism. Nat. Commun. 10, 3511.
Hughes, H.S.R., McDonald, I., Loocke, M., Butler, I.B., Upton, B.G.J., Faithfull, J.W., 2017. Paradoxical co-existing base metal sulphides in the mantle: The multi-event record preserved in Loch Roag peridotite xenoliths, North Atlantic Craton. Lithos 276, 103–121.
Jacobs, J., Pisarevsky, S., Thomas, R.J., Beckere, T., 2008. The Kalahari Craton during the assembly and dispersal of Rodinia. Precambrian Res. 160, 142–158.
Jagoutz, E., Dawson, J.B., Hoernes, S., Spettel, B., Wänke, H., 1984. Anorthositic oceanic crust in the Archean Earth. 15th Lunar Planet. Sci. Conf., pp. 395–396
Jugo, P.J., 2009. Sulfur content at sulfide saturation in oxidized magmas. Geology 37, 415–418.
Jugo, P.J., Wilke, M., Botcharnikov, R.E., 2010. Sulfur K-edge XANES analysis of natural and synthetic basaltic glasses: Implications for S speciation and S content as function of oxygen fugacity. Geochim. Cosmochim. Acta 74, 5926–5938.
Kamenetsky, V.S., Zelenski, M., 2020. Origin of noble-metal nuggets in sulfide-saturated arc magmas: a case study of olivine-hosted sulfide melt inclusions from the Tolbachik volcano (Kamchatka, Russia). Geology https://doi.org/10.1130/G47086.1.
Kamenetsky, V.S., Park, J.-W., Mungall, J.E., Pushkarev, E.V., Ivanov, A.V., Kamenetsky, M.B., Yaxley, G.M., 2015. Crystallization of platinum-group minerals from silicate melts: Evidence from Cr-spinel–hosted inclusions in volcanic rocks. Geology 43, 903–906.
Karup-Møller, S., Makovicky, E., 1995. The phase system Fe-Ni-S at 725° C. Neues Jahrbuch für Mineralogie, Monatshefte, pp. 1–10.
Kobussen, A.F., Griffin, W.L., O'Reilly, S.Y., 2009. Cretaceous thermo-chemical modification of the Kaapvaal cratonic lithosphere, South Africa. Lithos 112, 886–895.
König, S., Lorand, J.P., Luguet, A., Pearson, D.G., 2014. A non-primitive origin of near-chondritic S-Se-Te ratios in mantle peridotites; implications for the Earth's late accretionary history. Earth Planet. Sci. Lett. 385, 110–121.
König, S., Lissner, M., Lorand, J.P., Bragagni, A., Luguet, A., 2015. Mineralogical control of selenium, tellurium and highly siderophile elements in the Earth's mantle: evidence from mineral separates of ultra-depleted mantle residues. Chem. Geol. 396, 16–24.
Konzett, J., Armstrong, R.A., Gunther, D., 2000. Modal metasomatism in the Kaapvaal craton lithosphere: constraints on timing and genesis from U-Pb zircon dating of metasomatized peridotites and MARID-type xenoliths. Contrib. Mineral. Petrol. 139, 704–719.
Kutyrev, A.V., Kamenetsky, V.S., Sidorov, E.G., Abersteiner, A., Chubarov, V.M., 2020. Silicate inclusions in isoferroplatinum: Constraints on the origin of platinum mineralization in Ural-Alaskan type complexes. Ore Geol. Rev. 119, 103367.
Lawless, P.J., Gurney, J.J., Dawson, J.B., 1979. Polymict peridotites from the Bultfontein and De Beers mines, Kimberley, South Africa. In: Boyd, F.R., Meyer, H.O.A. (Eds.), The mantle sample. 2nd International Kimberlte Conference. American Geophysical Union, Washington, DC, pp. 145–155.
Lawley, C.J.M., Pearson, D.G., Waterton, P., Zagorevski, A., Bédard, J.H., Jackson, S.E., Petts, D.C., Kjarsgaard, B.A., Zhang, S., Wright, D., 2020a. Element and isotopic signature of re-fertilized mantle peridotite as determined by nanopowder and olivine LA-ICPMS analyses. Chem. Geol. 536, 119464.
Lawley, C.J.M., Petts, D.C., Jackson, S.E., Zagorevski, A., Pearson, D.G., Kjarsgaard, B.A., Savard, D., Tschirhart, V., 2020b. Precious metal mobility during serpentinization and breakdown of base metal sulphide. Lithos 354-355, 105278.
Le Roex, A.P., 1986. Geochemical correlation between southern African kimberlites and South Atlantic hotspots. Nature 324, 243–245.
Le Roex, A.P., Bell, D.R., Davis, P., 2003. Petrogenesis of group I kimberlites from Kimberley, South Africa: evidence from bulk-rock geochemistry. J. Petrol. 44, 2261–2286.
Le Vaillant, M., Barnes, S.J., Fiorentini, M.L., Miller, J., McCuaig, C., Muccilli, P., 2015a. A hydrothermal Ni-As-PGE geochemical halo around the miitel komatiite-hosted nickel sulfide deposit, Yilgarn Craton, Western Australia. Econ. Geol. 110, 505–530.
Le Vaillant, M., Barnes, S.J., Fiorentini, M.L., Santaguida, F., Törmänen, T., 2015b. Effects of hydrous alteration on the distribution of base metals and platinum group elements within the Kevitsa magmatic nickel sulphide deposit. Ore Geol. Rev. 72, 128–148.
Liu, Y., Brenan, J.M., 2015. Partitioning of platinum-group elements (PGE) and chalcogens (Se, Te, As, Sb, Bi) between monosulfide-solid solution (MSS), intermediate solid solution (ISS) and sulfide liquid at controlled fO2–fS2 conditions. Geochim. Cosmochim. Acta 159, 139–161.
Locmelis, M., Pearson, N.J., Barnes, S.J., Fiorentini, M.L., 2011. Ruthenium in komatiitic chromite. Geochim. Cosmochim. Acta 75, 3645–3661.
Lorand, J.P., Alard, O., 2010. Determination of selenium and tellurium concentrations in Pyrenean peridotites (Ariege, France): new insight into S/Se/Te systematics of the upper in mantle samples. Chem. Geol. 278, 120–130.
Lorand, J.P., Grégoire, M., 2006. Petrogenesis of base metal sulphide assemblages of some peridotites from the Kaapvaal craton (South Africa). Contrib. Mineral. Petrol. 151, 521–538.
Lorand, J.P., Luguet, A., 2016. Chalcophile and siderophile elements in mantle rocks: trace elements controlled By trace minerals. In: Harvey, J., Day, J.M.D. (Eds.), Highly Siderophile and Strongly Chalcophile Elements in High-Temperature Geochemistry and Cosmochemistry, pp. 441–488.
Lorand, J.P., Pattou, L., Gros, M., 1999. Fractionation of platinum-group elements and gold in the upper mantle: a detailed study in Pyrenean orogenic lherzolites. J. Petrol. 40, 957–981.

Lorand, J.P., Delpech, G., Grégoire, M., Moine, B., O'Reilly, S.Y., Cottin, J.Y., 2004. Platinum-group elements and the multistage metasomatic history of Kerguelen lithospheric mantle (South Indian Ocean). Chem. Geol. 208, 195–215.
Lorand, J.P., Luguet, A., Alard, O., Bezos, A., Meisel, T., 2008. Abundance and distribution of platinum-group elements in orogenic lherzolites; a case study in a Fontete Rouge lherzolite (French Pyrenees). Chem. Geol. 248, 174–194.
Lorand, J.P., Alard, O., Luguet, A., 2010. Platinum-group element micronuggets and refertilization process in Lherz orogenic peridotite (northeastern Pyrenees, France). Earth Planet. Sci. Lett. 289, 298–310.
Lorand, J.P., Luguet, A., Alard, O., 2013. Platinum-group element systematics and petrogenetic processing of the continental upper mantle: a review. Lithos 164, 2–21.
Luguet, A., Lorand, J.P., Alard, O., Cottin, J.Y., 2004. A multi-technique study of platinum group element systematic in some Ligurian ophiolitic peridotites, Italy. Chem. Geol. 208, 175–194.
Luguet, A., Shirey, S.B., Lorand, J.-P., Horan, M.F., Carlson, R.W., 2007. Residual platinum-group minerals from highly depleted harzburgites of the Lherz massif (France) and their role in HSE fractionation of the mantle. Geochim. Cosmochim. Acta 71, 3082–3097.
Maier, W.D., Peltonen, P., McDonald, I., Barnes, S.J., Hatton, C., Viljoen, F., 2012. The concentration of platinum-group elements and gold in southern African and Karelian kimberlite-hosted mantle xenoliths: implications for the noble metal content of the Earth's mantle. Chem. Geol. 302, 119–135.
Maier, W.D., O'Brien, H., Peltonen, P., Barnes, S.J., 2017. Platinum-group element contents of Karelian kimberlites: implications for the PGE budget of the sub-continental lithospheric mantle. Geochim. Cosmochim. Acta 216, 358–371.
Mallmann, G., O'Neill, H.S.C., 2009. The crystal/melt partitioning of v during mantle melting as a function of oxygen fugacity compared with some other elements (Al, P, Ca, Sc, Ti, Cr, Fe, Ga, Y, Zr and Nb). J. Petrol. 50, 1765–1794.
Mansur, E., Barnes, S.J., 2020. The role of Te, As, Bi, Sn and Sb during the formation of platinum-group-element reef deposits: Examples from the Bushveld and Stillwater Complexes. Geochim. Cosmochim. Acta 272, 235–258.
Mansur, E., Barnes, S.J., Duran, C.J., 2019. Textural and compositional evidence for the formation of pentlandite via peritectic reaction: Implications for the distribution of highly siderophile elements. Geology 47, 351–354.
Mavrogenes, J.A., O'Neill, H.S.C., 1999. The relative effects of pressure, temperature and oxygen fugacity on the solubility of sulfide in mafic magmas. Geochim. Cosmochim. Acta 63, 1173–1180.
McDonough, W.F., Sun, S.-S., 1995. The composition of the earth: chemical evolution of the mantle. Chem. Geol. 120, 223–253.
Menzies, M.A., Hawkesworth, C.J., 1987. Upper mantle processes and composition. In: Nixon, P.H. (Ed.), Mantle Xenoliths. John Wiley & Sons, Chichester, pp. 725–738.
Morrissey, L.J., Tomkins, A.G., 2020. Evaporite-bearing orogenic belts produce ligand-rich and diverse metamorphic fluids. Geochim. Cosmochim. Acta 275, 163–187.
Mungall, J.E., Brenan, J.M., 2014. Partitioning of platinum-group elements and Au between sulfide liquid and basalt and the origins of mantle-crust fractionation of the chalcophile elements. Geochim. Cosmochim. Acta 125, 265–289.
O'Reilly, S.Y., Griffin, W.L., 2013. Mantle metasomatism. In: Harlov, D.E., Austrheim, H. (Eds.), Metasomatism and the Chemical Transformation of Rock. Springer Verlag, Berlin Heidelberg, pp. 471–533.
Pagé, P., Barnes, S.J., 2016. The influence of chromite on osmium, iridium, ruthenium and rhodium distribution during early magmatic processes. Chem. Geol. 420, 51–68.
Pagé, P., Barnes, S.J., Bedard, J.H., Zientek, M.L., 2012. In situ determination of Os, Ir, and Ru in chromites formed from komatiite, tholeiite and boninite magmas: implications for chromite control of Os, Ir and Ru during partial melting and crystal fractionation. Chem. Geol. 302, 3–15.
Palme, H., O'Neill, H.S.C., 2005. Cosmochemical estimates of mantle composition. In: Holland, H.D., Turekian, K.K., Carlson, R.W. (Eds.), Treatise on Geochemistry. Elsevier Pergamon, Amsterdam.
Park, J.-W., Campbell, I.H., Eggins, S.M., 2012. Enrichment of Rh, Ru, Ir and Os in Cr spinels from oxidized magmas: evidence from the Ambae volcano, Vanuatu. Geochim. Cosmochim. Acta 78, 28–50.
Park, J.-W., Kamenetsky, V., Campbell, I.H., Park, G., Hanski, E., Pushkarev, E., 2017. Empirical constraints on partitioning of platinum group elements between Cr-spinel and primitive terrestrial magmas. Geochim. Cosmochim. Acta 216, 393–416.
Pattou, L., Lorand, J.P., Gros, M., 1996. Non-chondritic platinum-group element ratios in the Earth's mantle. Nature 379, 712–715.
Peach, C.L., Mathez, E.A., Keays, R.R., 1990. Sulfide melt silicate melt distribution coefficients for noble-metals and other chalcophile elements as deduced from MORB – implications for partial melting. Geochim. Cosmochim. Acta 54, 3379–3389.
Pearson, D.G., Wittig, N., 2014. The formation and evolution of cratonic mantle lithosphere – evidence from mantle xenoliths. In: Holland, H.D., Turekian, K.K. (Eds.), Treatise on Geochemistry. Elsevier Ltd., Amsterdam, pp. 255–292.
Pearson, D.G., Shirey, S.B., Harris, J.W., Carlson, R.W., 1998. Sulphide inclusions in diamonds from the Koffiefontein kimberlite, S Africa: constraints on diamond ages and mantle Re-Os systematics. Earth Planet. Sci. Lett. 160, 311–326.
Pearson, D.G., Irvine, G.J., Ionov, D.A., Boyd, F.R., Dreibus, G.E., 2004. Re-Os isotope systematics and platinum group element fractionation during mantle melt extraction: a study of massif and xenolith peridotite suites. Chem. Geol. 208, 29–59.
Peslier, A.H., Woodland, A.B., Bell, D.R., Lazarov, M., Lapen, T.J., 2012. Metasomatic control of water contents in the Kaapvaal cratonic mantle. Geochim. Cosmochim. Acta 97, 213–246.
Pokhilenko, N.P., 2009. Polymict breccia xenoliths: evidence for the complex character of kimberlite formation. Lithos 112, 934–941.
Rehfeldt, T., Foley, S.F., Jacob, D.E., Carlson, R.W., Lowry, D., 2008. Contrasting types of metasomatism in dunite, wehrlite and websterite xenoliths from Kimberley, South Africa. Geochim. Cosmochim. Acta 72, 5722–5756.
Richardson, S.H., Shirey, S.B., 2008. Continental mantle signature of Bushveld magmas and coeval diamonds. Nature 453, 910–913.
Richardson, S.H., Erlank, A.J., Harris, J.W., Hart, S.R., 1990. Eclogitic diamonds of Proterozoic age from Cretaceous kimberlites. Nature 346, 54–56.
Richardson, S.H., Shirey, S.B., Harris, J.W., Carlson, R.W., 2001. Archean subduction recorded by Re-Os isotopes in eclogitic sulfide inclusions in Kimberley diamonds. Earth Planet. Sci. Lett. 191, 257–266.
Richardson, S.H., Shirey, S.B., Harris, J.W., 2004. Episodic diamond genesis at Jwaneng, Botswana, and implications for Kaapvaal craton evolution. Lithos 77, 143–154.
Rielli, A., Tomkins, A.G., Nebel, O., Brugger, J., Etschmann, B., Zhong, R., Yaxley, G.M., Paterson, D., 2017. Evidence of sub-arc mantle oxidation by sulphur and carbon. Geoch. Perspect. Lett. 3, 124–132.
Rielli, A., Tomkins, A.G., Nebel, O., Raveggi, M., Jeon, H., Martin, L., Avila, J.N., 2018a. Sulfur isotope and PGE systematics of metasomatised mantle wedge. Earth Planet. Sci. Lett. 497, 181–192.
Rielli, A., Tomkins, A.G., Nebel, O., Brugger, J., Etschmann, B., Paterson, D., 2018b. Garnet peridotites reveal spatial and temporal changes in the oxidation potential of subduction. Sci. Rep. 8.
Righter, K., Campbell, A.J., Humayun, M., Hervig, R.L., 2004. Partitioning of Ru, Rh, Pd, Re, Ir, and Au between Cr-bearing spinel, olivine, pyroxene and silicate melts. Geochim. Cosmochim. Acta 68, 867–880.
Rohrbach, A., Ballhaus, C., Golla-Schindler, U., Ulmer, P., Kamenetsky, V.S., Kuzmin, D.V., 2007. Metal saturation in the upper mantle. Nature 449, 456–458.
Savelyev, D.P., Kamenetsky, V.S., Danyushevsky, L.V., Botcharnikov, R.E., Kamenetsky, M.B., Park, J.-W., Portnyagin, M.V., Olin, P., Krasheninnikov, S.P., Hauff, F., Zelenski, M.E., 2018. Immiscible sulfide melts in primitive oceanic magmas: evidence and implications from picrite lavas (Eastern Kamchatka, Russia). Am. Mineral. 103, 886–898.
Schmitz, M.D., Bowring, S.A., de Wit, M.J., Gartz, V., 2004. Subduction and terrane collision stabilize the western Kaapvaal craton tectosphere 2.9 billion years ago. Earth Planet. Sci. Lett. 222.
Shirey, S.B., Harris, J.W., Richardson, S.H., Fouch, M.J., James, D.E., Cartigny, P., Deines, P., Viljoen, F., 2002. Diamond genesis, seismic structure, and evolution of the Kaapvaal-Zimbabwe craton. Science 297, 1683–1686.
Shirey, S.B., Richardson, S.H., Harris, J.W., 2008. Mesoarchean to Mesoproterozoic Re-Os ages for sulfide inclusions in Orapa diamonds and implications for Kaapvaal-Zimbabwe craton development. 9th International Kimberlite, Frankfurt, Germany pp. 9IKC-A-00365, 02008.
Simon, N.S.C., Carlson, R.W., Pearson, D.G., Davies, G.R., 2007. The origin and evolution of the Kaapvaal cratonic lithospheric mantle. J. Petrol. 48, 589–625.
Tappe, S., Dongre, A., Liu, C.Z., Wu, F.Y., 2018. 'Premier' evidence for prolonged kimberlite pipe formation and its influence on diamond transport from deep Earth. Geology 46, 843–846.
Tassara, S., González-Jiménez, J.M., Reich, M., Schilling, M.E., Morata, D., Begg, G., Saunders, E., Griffin, W.L., O'Reilly, S.Y., Gregoire, M., Barra, F., Corgne, A., 2017. Plume-subduction interaction forms large auriferous provinces. Nat. Commun. 8, 843 (2017).
Tassara, S., Reich, M., Konecke, B.A., González-Jiménez, J.M., Simon, A.C., Morata, D., Barra, F., Fiege, A., Schilling, M.E., Corgne, A., 2020. Unraveling the effects of melt–mantle interactions on the gold fertility of magmas. Front. Earth Sci. 8, 29.
Taylor, W.R., 1998. An experimental test of some geothermometer and geobarometer formulations for upper mantle peridotites with application to the thermobarometry of fertile lherzolite and garnet websterite. Neues Jahrbuch Fur Mineralogie-Abhandlungen 172, 381–408.
Thomassot, E., Cartigny, P., Harris, J.W., Lorand, J.P., Rollion-Bard, C., Chaussidon, M., 2009. Metasomatic diamond growth: a multi-isotope study (^{13}C, ^{15}N, ^{33}S, ^{34}S) of sulphide inclusions and their host diamonds from Jwaneng (Botswana). Earth Planet. Sci. Lett. 282, 79–90.
Wainwright, A.N., Luguet, A., Schreiber, A., Fonseca, R.O.C., Nowell, G.M., Lorand, J.P., Wirth, R., Janney, P.E., 2016. Nanoscale variations in (OS)-O-187 isotopic composition and HSE systematics in a Bultfontein peridotite. Earth Planet. Sci. Lett. 447, 60–71.
Wang, Z., Chang, H., Zong, K.Q., Geng, X.L., Liu, Y., Yang, J., Wu, F., Becker, H., Foley, S., Yan Wang, C., 2020. Metasomatized lithospheric mantle for Mesozoic giant gold deposits in the North China craton. Geology 48, 169–173.
Wells, P.R., 1977. Pyroxene thermometry in simple and complex systems. Contrib. Mineral. Petrol. 62, 129–140.
Westner, K.J., Beier, C., Klemd, R., Osbahr, I., Brooks, N., 2019. In situ chalcophile and siderophile element behavior in sulfides from moroccan middle atlas spinel peridotite xenoliths during metasomatism and weathering. Minerals 9.
Wittig, N., Pearson, D.G., Baker, J.A., Duggen, S., Hoernle, K., 2010. A major element, PGE and Re-Os isotope study of Middle Atlas (Morocco) peridotite xenoliths: evidence for coupled introduction of metasomatic sulphides and clinopyroxene. Lithos 115, 15–26.
Wood, B.J., Kiseeva, E.S., 2015. Trace element partitioning into sulfide: How lithophile elements become chalcophile and vice versa. Am. Mineral. 100, 2371–2379.
Woodland, A.B., Koch, M., 2003. Variation in oxygen fugacity with depth in the upper mantle beneath the Kaapvaal craton, Southern Africa. Earth Planet. Sci. Lett. 214, 295–310.
Woodland, A.B., Girnis, A.V., Bulatov, V.K., Brey, G.P., Höfer, H.E., 2019. Experimental study of sulfur solubility in silicate-carbonate melts at 5-10.5 GPa. Chem. Geol. 505, 12–22.
Wu, F.-Y., Walker, R.J., Yang, Y.-H., Yuan, H.-L., Yang, J.-H., 2006. The chemical-temporal evolution of lithospheric mantle underlying the North China Craton. Geochim. Cosmochim. Acta 70, 5013–5034.
Wyatt, B.A., Lawless, P.J., 1984. Ilmenite in polymict xenoliths from Bultfontein and de Beers mines, South Africa. In: Kornprob, J. (Ed.), 3rd International Kimberlite Conference. Elsevier, Amsterdam, pp. 43–56.

Wykes, J.L., O'Neill, H.S.C., Mavrogenes, J.A., 2015. The Effect of FeO on the Sulfur Content at Sulfide Saturation (SCSS) and the Selenium Content at Selenide Saturation of Silicate Melts. J. Petrol. 56, 1407–1424.

Yaxley, G.M., Berry, A.J., Rosenthal, A., Woodland, A.B., Paterson, D., 2017. Redox preconditioning deep cratonic lithosphere for kimberlite genesis - evidence from the central Slave Craton. Sci. Rep. 7.

Zhang, H.F., Mattey, D.P., Grassineau, N., Lowry, D., Brownless, M., Gurney, J.J., Menzies, M.A., 2000. Recent fluid processes in the Kaapvaal Craton, South Africa: coupled oxygen isotope and trace element disequilibrium in polymict peridotites. Earth Planet. Sci. Lett. 176, 57–72.

Zhang, H.F., Menzies, M.A., Mattey, D.P., Hinton, R.W., Gurney, J.J., 2001. Petrology, mineralogy and geochemistry of oxide minerals in polymict xenoliths from the Bultfontein kimberlites, South Africa: implication for low bulk-rock oxygen isotopic ratios. Contrib. Mineral. Petrol. 141, 367–379.

Zhang, H.F., Menzies, M.A., Mattey, D., 2003. Mixed mantle provenance: diverse garnet compositions in polymict peridotites, Kaapvaal craton, South Africa. Earth Planet. Sci. Lett. 216, 329–346.